Institut Langevin
ONDES ET IMAGES

Plasmonic enhancement of single molecule emission in DNA origamis

Final internship report

Politecnico di Torino

Université Paris Cité

Candidate: Capuzzo Marco
Supervisor: Sébastien Bidault

Academic year 2023-2024

ESPCI PARIS | PSL

cnrs

Summary

a. Introduction

A crucial factor for developing fast single-photon emitters (SPEs) for quantum networks is enhancing the spontaneous emission decay rate, to obtain high photon count rates and to overcome dephasing, which suppresses photon indistinguishability [1]. Single photon emitters play a leading role in the functioning of quantum networks. The purpose is using the characteristics of the single photons, like the polarization and the spin, as the essential quantum bit of information: the qubit [2]. Single-photon emitters come in various forms, including color centers in diamond [3], single atoms [4], and quantum dots [5]. During my internship, single fluorescent organic molecules were used. The employed fluorophore ATTO647N is able to emit single photons in the red part of the visible spectrum, around 667 nm.

A pivotal point of single photon emitters is the working temperature. For many applications, cryogenic temperatures are required to limit the electron-phonon coupling and its consequent dephasing [6]. Emitters are then coupled to high quality microcavities to enhance their spontaneous emission rate using the Purcell effect and to render it faster than dephasing [7]. Nevertheless, working at cryogenic temperatures implies high costs and high operating powers. However, working at room temperature remains a challenge. This report discusses the feasibility of producing bright single photon sources outside of cryogenic conditions.

There are two key parameters which determine how a single photon emitter behaves, the decay rate and the above-mentioned dephasing rate. The first is linked to the population depletion from the excited state of the emitter, while the second is the rate at which the induced radiating electric dipole in the emitter loses coherence with respect to the excitation due to electron-phonon coupling. The aim is therefore to achieve a decay rate that is higher than the dephasing rate [8]. To achieve this goal, it is possible to decrease the dephasing rate and/or to speed up the decay from the excited state. In my work, I focused on increasing the decay rate through a plasmonic resonator cavity which surrounds the fluorophore. The parameter that provides a better description of the spontaneous emission enhancement is called the Purcell factor. It establishes a connection between the decay rate of the bare molecule with respect to the emitter coupled to a resonant cavity [9]. For this purpose, a single ATTO647N molecule is placed between two gold nanoparticles. In order to maximize the coupling strength, the resonance frequency of the gold nanoparticle dimer should be matched with the emission frequency of the fluorophore. Another important factor is the orientation of the transition dipole of the emitter [10]. When the molecular dipole is oriented along the dimer axis, the spontaneous emission is strongly enhanced. On the contrary when the two directions are perpendicular, the emission is strongly quenched [10].

The whole structure (figure 1a) is assembled around a DNA origami developed by Gaetan Bellot and his team in Montpellier, in which single strands of DNA are able to attach to the complementary strands on the functionalized gold nanoparticles. In figure 1b, it is possible to see the entire structure with the gold nanospheres covered by single strands of DNA and the DNA origami in the middle, which weakly interacts with the electron beam of the TEM. The length of the surface strands plays an important role in the resonance frequency but also in the stability of the structure. To redshift the resonance of the plasmonic nanostructure towards the resonance of the molecule, it is necessary to reduce the interparticle distance. Another parameter is the refractive index of the environment, which also modifies the

resonance frequency of the plasmonic dimer. In this report, we will use two ways to tune the resonance frequency of the nanocavity: by increasing the local ionic strength to bring the gold nanoparticles closer and by increasing the refractive index of the environment.

The chemical assembly of the structure composed by DNA origami and two gold nanoparticles is a delicate process, which requires optimizing the surface chemistry of the gold nanospheres (density and length of the surface DNA strands, addition of stabilizing ligands) and optimizing the ratio between gold nanospheres and DNA, which requires multiple purification steps as detailed in this report.

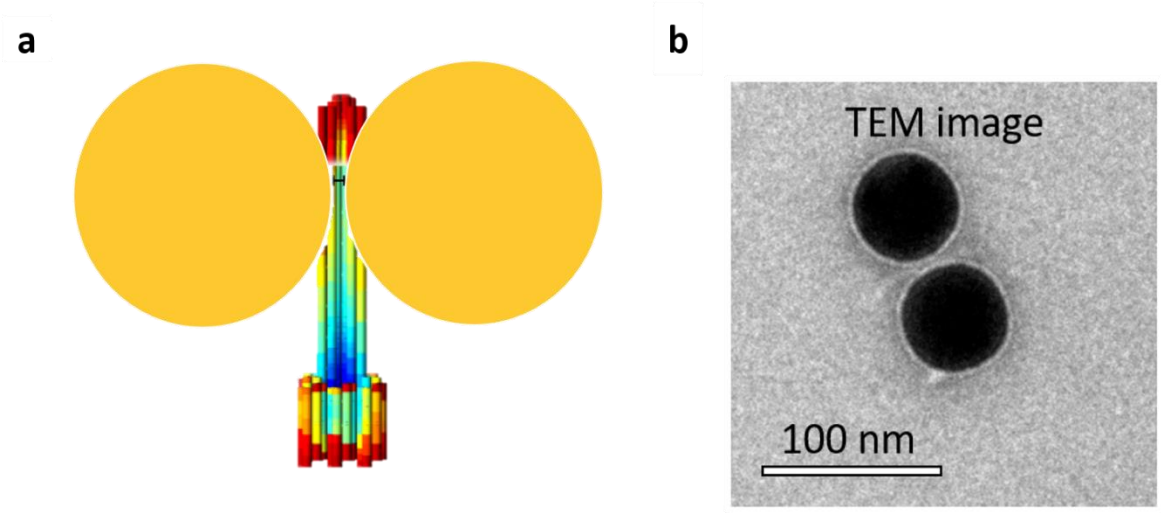

Figure 1 a) Assembled-structure with a DNA origami scaffold which assembles two 60 nm diameter gold nanospheres b) TEM image of the assembled-structure. Gold atoms scatter strongly the incoming electrons while the DNA origami between the particles appears lighter than the environment, which was stained with a uranyl complex to slightly interact with the electron beam.

The optical characterization of the assembled nanostructures is performed by analysing both the elastic scattering and inelastic fluorescence provided by single nanostructures. The analysis of darkfield scattering images allows us to observe the assembled dimers and to acquire their scattering spectra to infer their resonance wavelength. Alternatively, by performing a fluorescence analysis, it is possible to measure the excited state lifetime of single molecules, allowing the calculation of the Purcell factor. One of my main contributions during my internship was to correlate both techniques on the same plasmonic dimer, achieving a complete optical characterization of the coupled nanostructure.

During my internship, I worked on all aspects of the project: chemical assembly, optical characterization, simulations and data analysis.

b. Presentation of the lab and of the team

My internship took place at the Institut Langevin – Ondes et images of Paris in the 5th arrondissement. It is only a few metres away from the Campus Pierre-et-Marie-Curie and from Jardin des Plantes. The Institute features several groups with different fields of interest like the study of mechanical, acoustic but also electromagnetic waves, as in the case of my

internship. My team is coordinated by Dr. Sebastien Bidault who is also one of the two coordinators of the "Subwavelength physics (SWAP)" theme of the Institut. During my internship, I was also supervised by a third-year PhD student, Claudia Corti. Moreover, I gave and received advice from another master 2 intern working with Sebastien Bidault, Zixiao Zhang, since both our projects tackled the assembly of plasmonic nanostructures on DNA origamis (for biosensing in the case of Zixiao's internship). Furthermore, Gaetan Bellot and his team from CBS in Montpellier engineered the DNA origami tower design and I joined two zoom meetings with his team. The gold nanospheres used during my internship were synthesized by Sylvie Marguet from NIMBE, CEA Saclay.

c. Theoretical background

i. Single molecules as single-photon emitters

The single photon emitter in my work is the organic fluorophore ATTO647N, which absorbs around 647 nm and emits around 667 nm. At 0 K, a quantum emitter can be described as a two-level system, the ground state |g> and the excited state |e>, and it is excited when the incoming photons match precisely the energy difference between states. At room temperature, it is necessary to consider vibrational sublevels for both electronic states and the system is well described by the Jablonski diagram in figure 2.

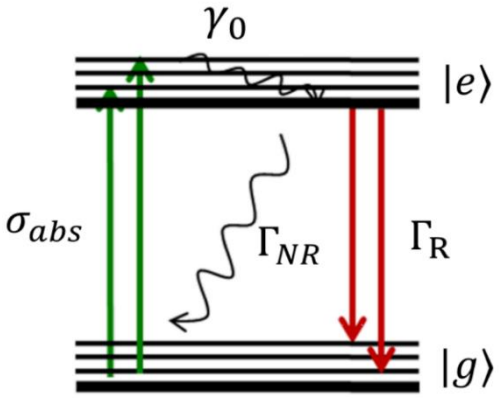

Figure 2 Fluorophore's Jablonski diagram. The electron in the ground state|g> is stimulated to the excited state |e> with an absorption cross section σ_{abs}. The two states present different levels due to the coupling with the vibrational states. The electrons can dephase non-radiatively with a γ_0 rate. The deexcitation from|e> to |g> may happen radiatively (Γ_R) or non-radiatively (Γ_{NR}).

In these conditions, there is a thermal broadening of the states, due to the coupling with vibrational states. Because of this phenomenon, the absorption spectrum of the fluorophore becomes broader, typically by 6 orders of magnitude, lowering the excitation cross-section of the emitter by the same factor. This allows photons with slightly higher energies than the exact energy difference to still excite the electron to the |e> state, although with a lower probability for energies further away from the ideal value. When the emitter is in its excited state, it undergoes very fast non-radiative dephasing (γ_0), in the order of several tens of femtoseconds, until it reaches the fundamental vibrational level and the electronic excited state. The main consequence of this dephasing is that there is a loss in coherence between

the induced dipole in the emitter and the incoming excitation field. After this relaxation process, the electron is at a lower energy, implying that the eventual emitted photon is less energetic. The difference between excitation and emission wavelengths is called Stokes shift. At this point the excited emitter can relax both in a non-radiative or in a radiative way [11]. The average time spent by an electron in the excited state is called the fluorescence lifetime (the inverse of the rate $\Gamma=\Gamma_R+\Gamma_{NR}$) which, for fluorescent molecules, is typically in the nanoseconds to picoseconds range [12]. The purpose of my internship is to investigate by how much we can reduce the fluorescence lifetime, since we are interested in the development of single-photon emitters with a high rate of photons emitted per second and with a decay rate as close as possible to the dephasing rate [7]. The challenge is to achieve good results at room temperature, where the interaction cross-section between light and matter is reduced of 6-7 order of magnitude due to the electron-phonon coupling [13].

The quantum yield of fluorophores is another significant coefficient to consider. It is defined as the probability of an excited molecule to emit photons when it is in the excited state. Another way to express it is by the fraction of excited state that decay radiatively with respect to the total $\phi_0 = \Gamma_{R0}/\Gamma_0$ (with $\Gamma_0 = \Gamma_{R0} + \Gamma_{NR0}$). The 0 subscript describes the molecule without the plasmonic resonator. The quantum yield varies between 0 to 1 and the higher it is, the higher is the efficiency of the single photon source.

Another important factor that must be considered is the fluorescence intensity. For a bare emitter in position *r*, oriented along u_p is generally described as a photon flux integrated on a collection angle (Ω), centered at ω_{fluo} which is the emission wavelength:

$$I_{fluo}(\omega_{exc}, \omega_{fluo}, \Omega, r, u_p) = \eta_{collec}(\omega_{fluo}, \Omega, r, u_p) \times \sigma_{abs}(\omega_{exc}) \times |E_0(\omega_{exc}, r).u_p|^2 \times \phi_0$$

Where η_{collec} is the collection efficiency of the optical setup, σ_{abs} is the absorption cross-section, E_0 is the field amplitude at the emitter position and ϕ_0 is the emitter quantum yield.

ii. Plasmonic resonators

In this work, metallic nanoparticles are used as a resonant nanocavity, allowing an enhancement of the emission rate of the fluorophore using the Purcell effect [14]. When light strikes noble metal nanoparticles at the right wavelength, a phenomenon called Localized Surface Plasmon Resonance (LSPR) occurs [15]. This phenomenon causes the electrons within the nanoparticles to move collectively, creating a high localized electromagnetic field around the particle. It is possible to analyse the interaction between light and metallic nanoparticles using different approximations. The easiest one is the quasi-static approximation, in which it is assumed that the size of the nanoparticles is extremely small with respect to the radiation wavelength [16]. In this framework, the nanoparticle acts only as an induced dipole which oscillates at the same frequency as the incident radiation. This model works well for metallic particle sizes below 20 nm, giving also a volume-independent value of the resonance at $\mathrm{Re}(\varepsilon_p) = -2\varepsilon_{ext}$ in the case of spherical particles, where ε_p and ε_{ext} are respectively the dielectric constant of the nanoparticle and of the environment. So, the real part of the dielectric constant should be negative, as in noble metals like gold [17]. Figure 4e, 4f provide experimentally measured values of real and imaginary parts of the dielectric constant of gold

[18]. We observe indeed that the real part of the dielectric index for gold is negative in the visible range. Using the quasistatic resonance condition, these data explain the resonance of small gold particles in the green part of the spectrum, appearing red in transmission [19]. Furthermore, the imaginary part of the experimental dielectric function presents a dip near 650 nm, meaning that, working at those frequencies, the absorption in gold is minimized. This is why the fluorophore was chosen with a resonance close to this frequency. To tune the resonance from the green to the red part of the spectrum, we will use particle dimers instead of single spheres.

If an exact solution of the problem is required for a spherical particle, it is possible to use Mie theory [20] [21], in which Maxwell's equations are analytically solved. This theory can be extended for multiple spheres at the cost of high mathematical complexity. For this reason, during my internship, I simulated the optical response of nanosphere dimers using a finite element method developed by F. J. Garcia de Abajo et A. Howie which has been implemented as a numerical tool called MNPBEM [22][23][24] (Metallic Nanoparticle Boundary Element Method). In this framework, the nanoparticle surfaces are meshed to solve the boundary conditions of Maxwell's equations. Compared to Mie theory, this simulation framework has the strong advantage of being compatible with non-spherical shapes. Furthermore, many parameters can be tuned such as the refractive index of the media, the orientation of the dipole, the size of the nanoparticles and the possibility to add other nanoparticles at certain distances. This last feature is very important for our work since we want to compare the experimental result of the dimers with the simulated ones.

By arranging two nanoparticles close to each other, the induced electromagnetic fields that they produce interact in the near-field with a consequent change in resonance of the coupled system, as we can see from the scattering cross section in figure 4b. Qualitatively, we can consider the nanoparticles as induced dipoles which interact together, generating an interparticle coupling. The two resonant nanoparticles are no longer independent from each other, giving rise to a hybridization of their dipolar modes [25]. As we can see from figure 3, this gives rise to three quadrupolar modes that are neglected for their weak interaction with light (so-called dark modes) and three dipolar modes that are bright: the longitudinal mode, when the induced dipoles are parallel to the dimer axis, and the two degenerate transverse modes, when the induced dipoles are perpendicular to the axis. These modes thus provide two new hybrid resonances, similarly to the hybridization of *p* orbitals in molecules (leading to π and σ bonds). The lowest in energy is the parallel case, where the induced dipoles are cooperatively coupled, meaning that the positive area of a dipole is close to the negative one of the other dipole. If the dipoles are not parallel but in perpendicular configuration, more energy is required for the excitation. This is due to the noncooperative interaction between the two induced dipoles and it also implies higher excitation energies for smaller interparticle distance (blueshift). Since the longitudinal mode is cooperative, it corresponds to an induced coupled dipole that is significantly larger than for the transverse modes: this is why the optical response of nanosphere dimers is dominated by the longitudinal mode and why we will only consider this mode for the rest of the report.

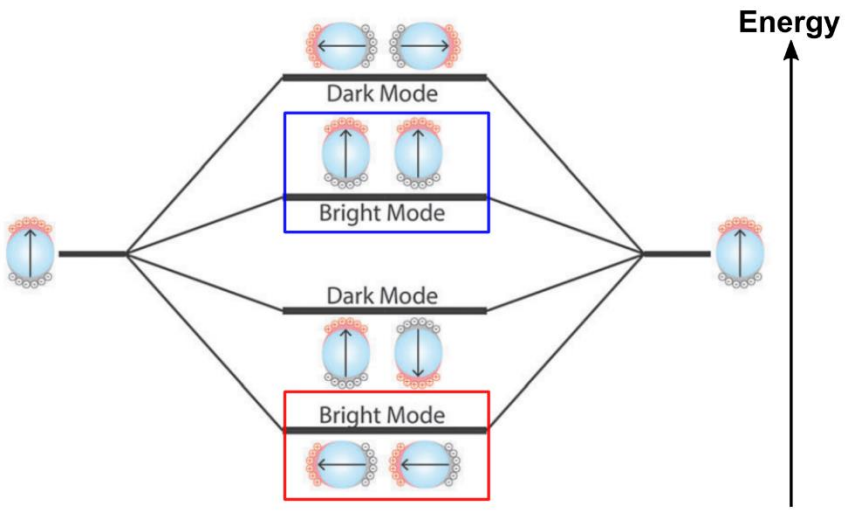

Figure 4 Hybridization of two resonators.

Furthermore, when the longitudinal mode is excited, the field enhancement in dimers is orders of magnitude larger than for single spheres and the field is confined in a very small volume, called a hot-spot [26] [27], as we can see in figure 4d.

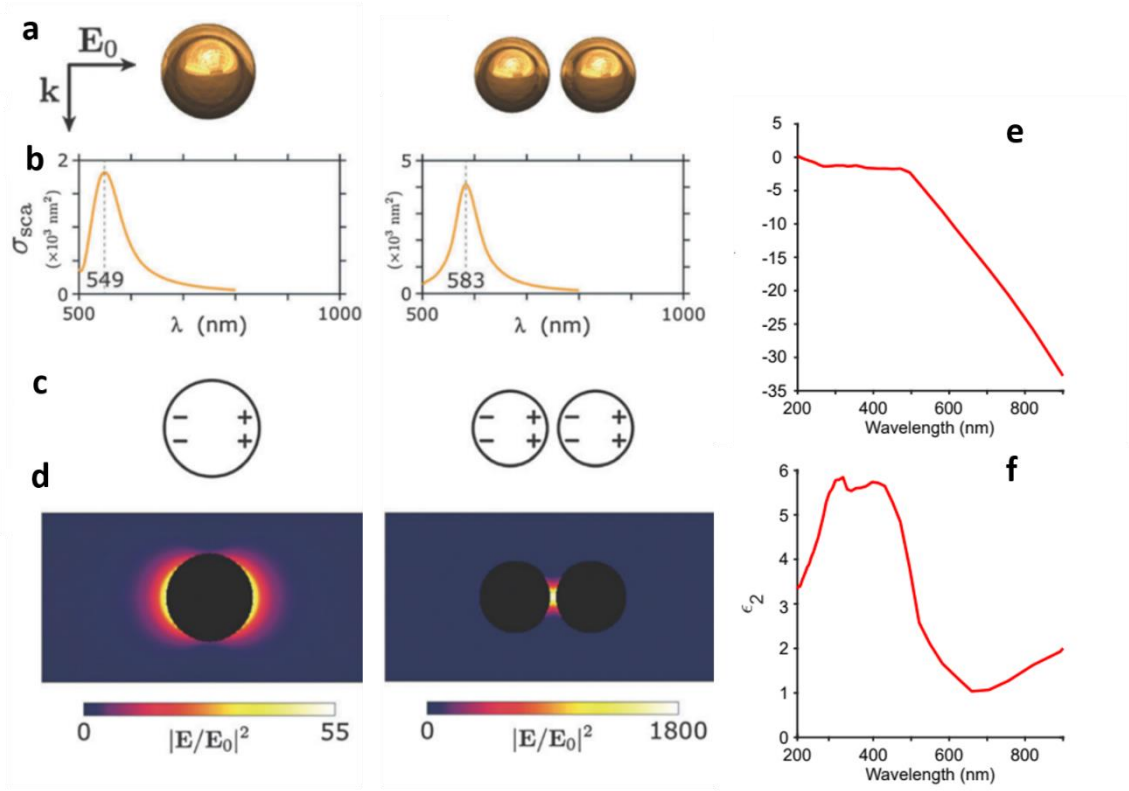

Figure 5 a) Nanoparticles scheme b) Scattering cross sections c) Charges distribution d) Electromagnetic field enhancement obtained by simulations [26] e\f) Gold's dielectric function obtained experimentally e) Real part f) Imaginary part

As we will see later in this report, it is possible to control the distance between the two nanoparticles by decreasing the electrostatic repulsion between the spheres due to the

negative DNA functionalized surface by increasing the ionic strength of the environment. The DNA single strands which cover the nanoparticles surface limit the gold nanoparticles from getting closer. By increasing the number of positive ions, the DNA single strands are neutralized and forced to collapse, allowing the gold nanoparticles to approach. In this way the parallel longitudinal mode undergoes a redshift. The idea is to redshift the coupled-resonators frequency towards the fluorophore emission frequency.

iii. Enhancing spontaneous emission in plasmonic resonators

The structure composed by two gold nanospheres acts as a resonant cavity for the ATTO647N emitter located in the middle of the DNA origami structure. The purpose is to reach a large Purcell factor, which is a figure of merit of how much the spontaneous emission decay rate of the cavity-emitter structure is increased with respect to the bare emitter's one. By modifying the environment of the emitter, both the excitation and emission are affected. The excitation is enhanced due to the enhancement of the incoming field in the centre of the dimer. Meanwhile the emission is affected owing to an increase in the local density of optical states.

Between resonator and emitter, two regimes of coupling can occur: the weak coupling [28] and the strong coupling [29]. In weak coupling, the emission properties change without changing the resonance frequency, while, in strong coupling case, the resonance frequency is also affected, since the difference between the energy levels changes. In the current report, all experiments remain in a weak coupling regime.

In summary, the emission properties of an emitter depend both on intrinsic properties but also on the electromagnetic environment. In the weak coupling regime, the probability of transition from an excited eigenstate $|e\rangle$ to the ground state $|g\rangle$, localized in r_0 with a dipole moment μ_{01}, is described by Fermi's golden rule, as a result of a weak perturbation:

$$\Gamma = \frac{\omega}{\epsilon_0 \hbar} |\mu_{01}|^2 \rho_p(r_0, \omega)$$

Where ρ_p (r_0, ω) is the local density of optical states, which gives the information on the number of channels in which our emitter in r_0 can deexcite. This last term is crucially affected by the presence of a resonant cavity, which increases the number of optical states. Consequently, the excited dipole has many ways to radiatively or non-radiatively deexcite, implying a reduction in the lifetime. Importantly, the Purcell factor depends on the variation of the local density of optical states when we add a resonant cavity.

By considering the case where just one mode is confined, the Purcell factor will have the following form:

$$F_p = \frac{\Gamma_{tot}}{\Gamma_0} = \frac{3Q}{4\pi^2} \frac{\lambda^3}{V_m}$$

Where Q is the resonator's quality factor and V_m is the mode volume. By approaching two gold nanospheres, the electric field is enhanced and confined in a smaller volume.

The electromagnetic environment modification due to the plasmonic resonator also changes the number of deexcitation channels, both radiative and non-radiative. We can express a modified quantum yield as:

$$\phi = \frac{\Gamma_R}{\Gamma_R + \Gamma_{NR} + \Gamma_{NR0}}$$

Where Γ_R is the radiative decay rate of the coupled emitter-resonator system and Γ_{NR} describes the extra non-radiative decay channels introduced by the plasmonic resonator. By increasing the radiative channels more than non-radiative ones, we get an increase in ϕ. Inversely, if the non-radiative deexcitation is dominant, a decrease in the spontaneous emission takes place. This phenomenon is called *quenching* [11]. If the emitter is efficiently coupled with a resonator, Γ_R and Γ_{NR} will be larger than Γ_{NR0}. In this case the final fluorescence quantum yield will be independent from the initial quantum yield.

The presence of the plasmonic resonator around the fluorophore, influences also the intensity of the spontaneous emission. Therefore, the intensity enhancement due to the plasmonic nanostructure will be:

$$\frac{I_{fluo-ant}(\omega_{exc}, \omega_{fluo}, \Omega, r, u_p, R)}{I_{fluo-ref}(\omega_{exc}, \omega_{fluo}, \Omega, r, u_p)} = \frac{\eta_{ant}(\omega_{fluo}, \Omega, r, u_p, R)}{\eta_{ref}(\omega_{fluo}, \Omega, r, u_p)} \times \frac{|E_{local}(\omega_{exc}, r, R).u_p|^2}{|E_0(\omega_{exc}, r).u_p|^2} \times \frac{\phi(r, u_p, R)}{\phi_0}$$

Basically, the plasmonic nanostructure cavity acts on two factors; firstly, it affects the absorption probability which is proportional to the intensity of the electric field parallel to the transition dipole of the emitter, in the emitter position; secondly it acts on the quantum yield since the presence of the resonators generates new deexcitation channels, both radiative and non-radiative. Plasmonic resonators can also strongly influence the collection efficiency but this is not the case for nanosphere dimers which essentially radiate like an induced dipole, similarly to an isolated molecule. From this formula, we can see that a strong electric field enhancement will only allow for fluorescence intensity enhancement if the quantum yield of the emitter is not too reduced compared to the bare molecule. It also shows that, for a fixed field enhancement and since the final quantum yield is dominated by the radiative yield of the plasmonic resonator, the intensity enhancement is much larger for initially “bad” emitters (small ϕ_0) than for good ones (ϕ_0~1).

The reciprocity theorem of electromagnetism implies that a resonator that can enhance the reception of a wave by an electric dipole will also allow the dipole to radiate the same frequency more intensely in the far field. In the case of quantum emitters [30], this theorem provides a relationship between the enhancement of the local electromagnetic field and the change in the radiative deexcitation rate:

$$\frac{|\mathbf{u}_p.\mathbf{E}_{local}(\omega_{exc}, r, R)|^2}{|\mathbf{u}_p.\mathbf{E}_0(\omega_{exc}, r)|^2} \sim \frac{\Gamma_R}{\Gamma_{R0}} \frac{\eta_{ant}(\omega_{fluo}, \Omega, r, \mathbf{u}_p, R)}{\eta_{ref}(\omega_{fluo}, \Omega, r, \mathbf{u}_p)}$$

This formula implies that a resonator that is able to strongly enhance the local electromagnetic field will also provide a large radiative component of the Purcell factor [31] [32] (especially since collection efficiency effects can be neglected for nanosphere dimers). It also means that if fluorescence intensity enhancements and Purcell factors are very different, then it means that non-radiative channels are probably dominant. If the fluorescence intensity

enhancement is much larger than the Purcell factor, it probably means that the emitter was initially bad (ϕ_0~0). If the fluorescence intensity enhancement is much smaller than the Purcell factor, than it means that the final quantum yield is low ($\phi << \phi_0$) and that non-radiative decay channels dominate in the reduction of the excited state lifetime.

d. State of the art and objectives of the project

The first experimental demonstration of the modification of the spontaneous emission decay rate of an emitter due to the electromagnetic environment was realized by Drexhage in 1966. In this work, the scientists studied the lifetime of the emitter in function of the distance with a silver mirror [33]. The enhancement of the fluorescence at room temperature thanks to plasmonic structures has been widely studied in different ways. One of the first experiments at room temperature with a gold nanosphere has been performed with an Atomic Force Microscopy (AFM) [34] [35] . The idea was to place the nanoparticle on the tip of the AFM in order to control the distance between the emitter and the plasmonic structure.

One of the most used methods for the fabrication of plasmonic nanostructure is lithography. In the work of Kinkhabwala et al. [36], they demonstrated that it was possible to decrease the lifetime of the spontaneous emission by employing nanotriangles aligned along the tips (figure 5a). This configuration allows a strong electromagnetic field confinement which enhances the excitation of the longitudinal polarization along the axes of the dimers. The lithographic approach allows to control the interparticle distance but also to control the shape and the orientation of the nanostructures. The drawback is the random placement of the emitter, giving a large distribution of lifetimes. However, this work has reached a lifetime enhancement up to a factor of 25. Other works have shown that is possible to control the position of the emitters by implementing a complex multi-step lithographic process [37] [38].

Another possibility is to use nanotechnologies based on DNA, since they allow to control the number of emitters and their positioning with respect to the plasmonic nanostructure. The assembly of the structures can be done by employing a simple DNA double-strand [39] [40] [41] [42] but also by using more complex structures called DNA origamis [43] [44] [45] [46]. The group of Sebastien Bidault has used the first method. Firstly, it has been investigated the auto-assembly with a DNA double-strand with a single molecule placed in the middle of the strand. In this work, it was demonstrated that this implementation allows to decrease the lifetime of the emitter by more than 2 orders of magnitude (figure 5b), while fluorescence increases, up to nearly 2 orders of magnitude, when increasing the size of the plasmonic nanospheres, implying an enhancement of local field without reducing the quantum yield [42] (figure 5c).

A DNA origami is a self-assembled nanostructure based on a complex DNA folded structure for nanotechnology applications [47]. The backbone of the DNA origami is composed by a long viral DNA single-strand called scaffold strand, on which shorter single-strands are able to hybridize through specific base-base pairing, forcing the scaffold strand to fold in the desired way [48]. The specificity of the binding is ensured by the different base sequences of the single strands, which are complementary to certain sequences in the DNA scaffold strand. The final structure is self-assembled just by mixing together the scaffold strand with the staple strands

in certain conditions [49]. This technology allows to build specific nanostructures with a nanometer-level control [47], resulting in a powerful tool for many applications like drug delivery [50] and molecular sensing [51].

Another group, Tinnefeld, Acuna & coworkers [44], worked on the fluorescence intensity enhancement in plasmonic dimers based on DNA origamis. In this study, they analysed the influence of the initial quantum yield, underlining the importance of the electromagnetic field enhancement at the emitter position. They used a pillar-like DNA origami structure which allows to attach two 100 nm gold nanospheres at a 12 nm distance (figure 7a). They studied the fluorescence intensities at different $NiCl_2$ concentrations, where the salt acts as a quencher which decreases the quantum yield of the emitter. They demonstrated that the quenched molecule presented a fluorescence emission enhancement up to 5000, much more than the non-quenched case which reached up to 100.

In brief, in self-assembled plasmonic resonators, enhancement factors of about two orders of magnitude can be achieved for both the emission decay rates and the intensity enhancement (and more than three orders for the intensity when quenching the emitter). While such enhancement factors are exciting to detect single molecules at high concentrations [44] or to image them using a simple smartphone camera instead of costly scientific cameras [18], they are insufficient for coherent single photon emission. DNA origami structure used by K. Trofymchuk *et al.* is reported in figure 7b.

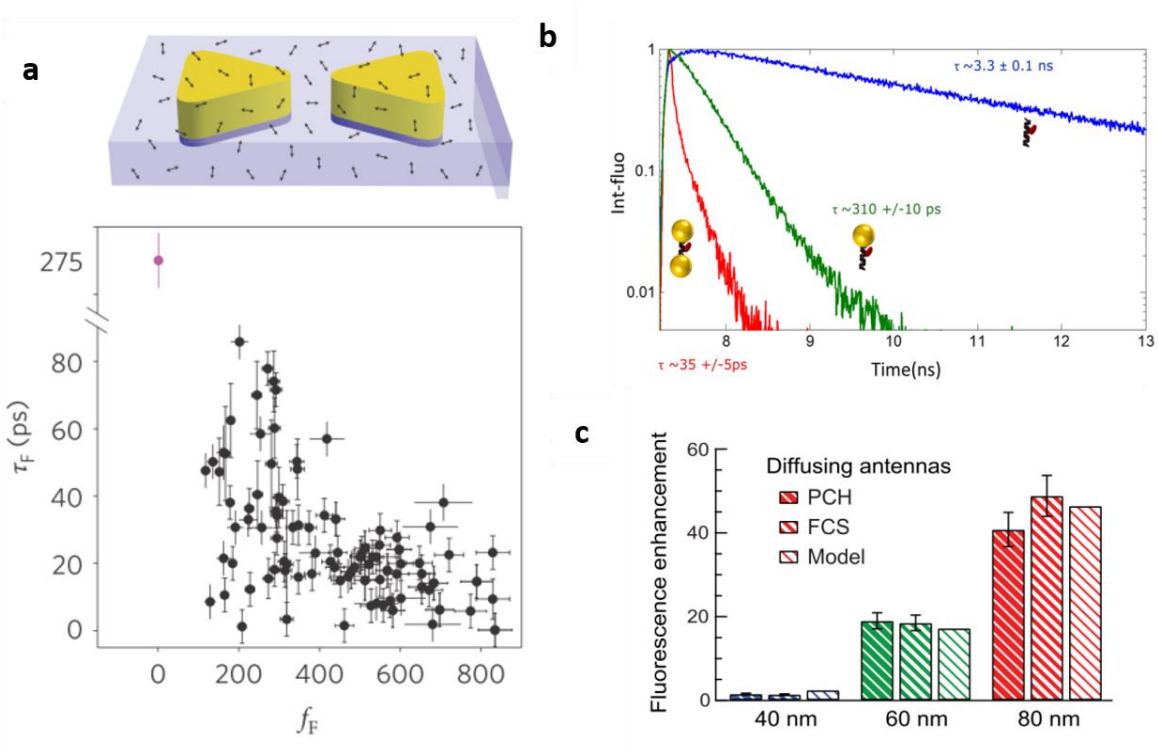

Figure 5 a) on top: nanotriangles disposition in Kinkhabwala et al. work with many molecules randomly positioned. On bottom: wide lifetime distribution due to the inability of molecules' position control. b) Lifetime comparison between assembled-structure (red), semi assembled-structure (green) and single ATTO647N (blue) in [41] c) Average fluorescence enhancement of ATTO647N between two gold nanospheres of 40 nm (blue), 60 nm (green) and 80 nm (red) of diameter. From [42].

To achieve coherent photon emission at room temperature, a key challenge is maintaining

coherence in the excited state. This necessitates a spontaneous emission rate (Γ) exceeding the dephasing rate (γ_o). The dephasing is in the order of several tens of femtoseconds and the bare molecule spontaneous emission decay rate is ~4 ns, so in order to have Γ faster than γ_o, we need a Purcell factor in the order of 10^5. In this way, one can hope to produce indistinguishable single photons. In my work, I concentrated my attention on enhancing the Purcell factor by ensuring also a high emission quantum yield to produce bright emitters. We can see from figure 6, rearranged from Heintz et al. [52] [53], that 60 nm gold nanospheres can provide a maximum Purcell factor close to 10^5 and a good quantum yield for a spacing around 3 nm. Reducing the gold nanosphere size to 40 nm increases the Purcell factor due to stronger electromagnetic field confinement but it implies also a strong quantum yield reduction. Then, it is possible to exploit the lightning rod effect at the tips of anisotropic particles by considering an emitter positioned between the tips of two plasmonic nanocubes. We notice that for dimers of 40 nm gold cubes or 30 nm silver cubes, a further increase in the Purcell factor is achieved while maintaining an expected quantum yield similar or larger than the one for dimers of 60nm gold nanospheres. These simulations were performed with the dipole aligned along the axis of the dimer. However, dimers of silver or gold nanocubes cannot be aligned using a simple DNA double strand as used in the previous work performed in the group of S. Bidault [41]. However, DNA origamis are capable of assembling anisotropic particles with an excellent control over their relative orientation [54]. Also, it was recently demonstrated that DNA origamis can be used to align single molecules with a chosen orientation [55]. All of these considerations justify the choice of a DNA origami to produce well-defined plasmonic cavities.

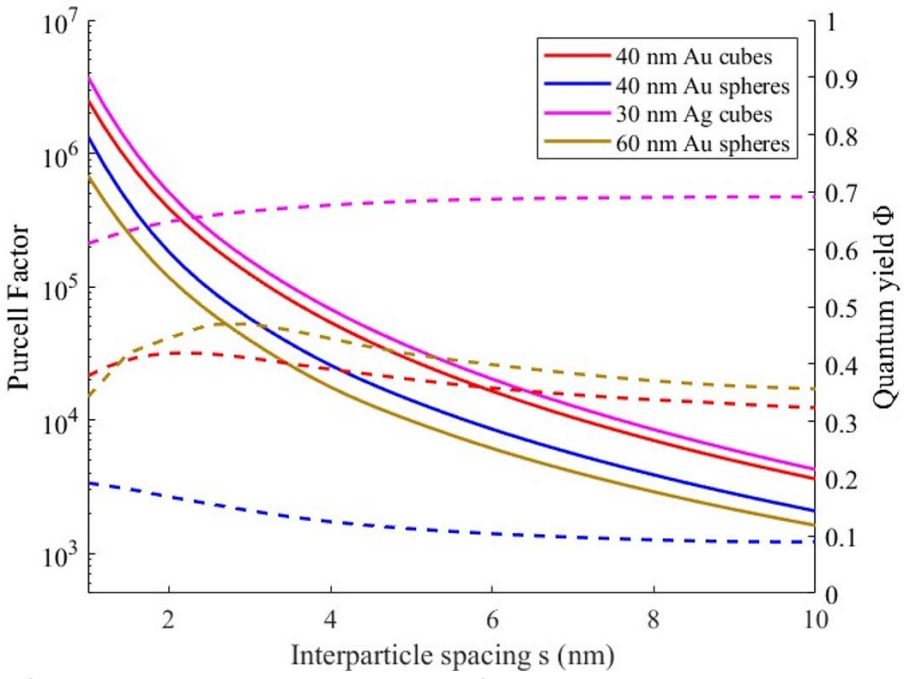

Figure 6 Purcell factor and quantum yield comparison for a single emitting dipole in the centre of dimers of 40 nm gold nanospheres (blue), 60 nm gold nanospheres (green), 40 nm gold nanocubes (red) and 30 nm silver nanocubes (magenta). Rearrangement from [52] & [53].

During my internship I focused my attention on 60 nm gold nanospheres, with the future perspective of using 40 nm gold nanocubes with a different DNA origami. Then it is very promising to adjust the chemical assembly procedure in order to work with silver nanocubes, since they present the largest Purcell factor and the largest quantum yield.

In our work, we employed a pillar-like DNA origami structure (figure 7c), similar to the one used by Tinnefeld, Acuna & coworkers, with the possibility to attach two DNA functionalized gold nanospheres, thanks to DNA binding. The DNA origami accommodates the dye molecule ATTO647N exactly between the gold nanospheres, in order to exploit the maximum field enhancement. These structures are designed and provided by G. Bellot at CBS in Montpellier, expert in DNA architectures design [56] [57].

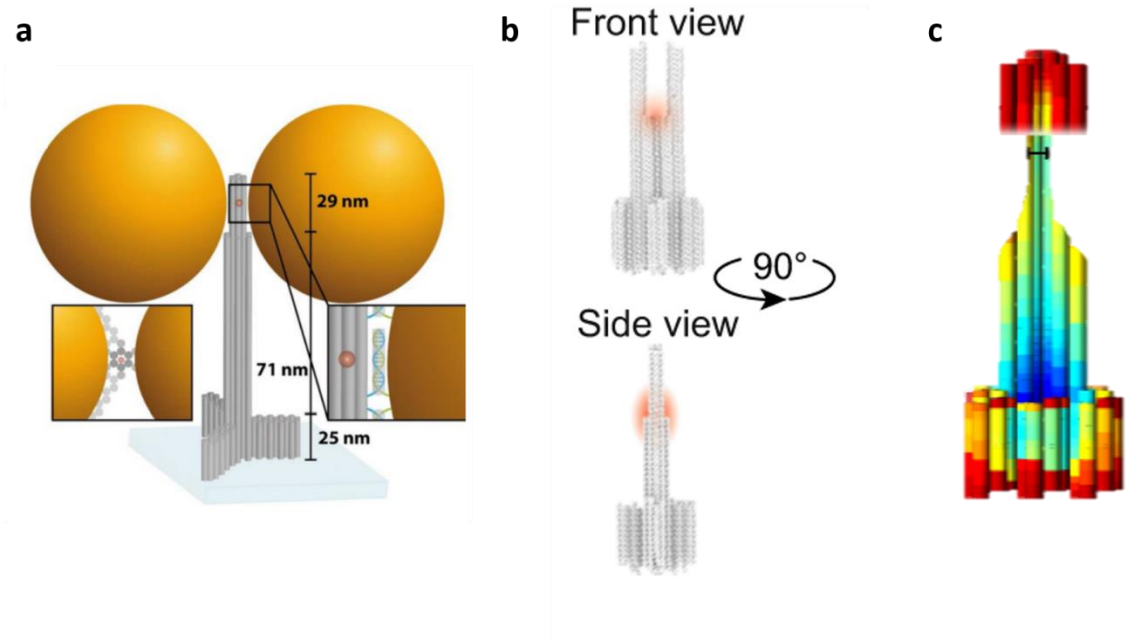

Figure 7 DNA origami structures. a) DNA origami structure in [44] b) Double-pillar DNA origami with a gap in the hot spot, from [46] c) DNA origami pillar for nanospheres employed by our group. Engineered by G.Bellot & coworkers at CBS in Montpellier

e. Methods

i. Chemical assembly

The dimer structure composed by the DNA origami linked to two gold nanoparticles through complementary DNA strands is synthesized over a three days period. At the end, the purpose is to obtain a sample with a high dimer concentration and with a high dimers/monomers ratio. For this purpose, the sample is subjected to two cycles of electrophoresis purification.

On the first day, the goal is to functionalize the nanoparticles with thiolated DNA single-strands. First of all, the length of the single DNA strands must be chosen. A trade off must be found between long strands and short strands. The shorter the strand is, the shorter the ligand shell will be, allowing the particles to be closer, but, at the same time, the colloidal stability of

the particles is lower with the risk of aggregating them in the presence of Mg^{2+} ions, which are necessary for the stability of the DNA origamis. Inversely, longer strands allow a higher colloidal stability and a more stable double-stranded link with the origami, but at the cost of forbidding the particles to get as close as possible. It is possible to employ a mix of shorter and longer strands: the idea is to minimize the size of the ligand shells while providing long DNA strands to link with the origami. The purpose of getting the nanoparticles close enough is for the dimer to resonate at the emission wavelength of the fluorophore, enhancing in this way the spontaneous emission.

The single DNA strands are composed of a chain of thymine bases and of a trithiol group. The choice of thymine bases is to avoid non-specific interaction with the gold surface and to ensure the ligands are accessible to the DNA origami [58]. The trithiol group is found on one of the extremities, allowing a covalent bond to the surface of the gold nanospheres [59]. In order to activate the trithiol (*i.e.* to insure it is not oxidized and therefore inactive to link with gold), the DNA strands are first incubated for two hours with a mild reducing phosphine molecule. In parallel, the CTAB covered 60 nm gold nanospheres are concentrated by centrifugation to reach a ~$2.5*10^{12}$ part/µL concentration in a 12 µL volume. At this point the nanoparticles and the DNA strands are mixed to replace the CTAB layer by the DNA shell. The first step is to add a surfactant to minimize particle aggregation (TWEEN 20 at ~300 mM concentration), followed instantaneously by hydrochloric acid, which neutralizes the DNA backbone at a pH close to 1 [60] in order to allow it to reach the nanoparticle surface to form a thiol-gold bond. After five minutes of incubation, a tris-borate-EDTA (TBE) buffer solution is added to bring back the pH to neutral levels. At the end, the sample is put in the rotator mixer all night long to maximize the density of DNA ligands on the particle surface.

On day two, after having rinsed the sample with TBE and subjected it to a cycle of centrifugation to remove leftover reactants, an amphiphilic thiolated alkyl-ethylene glycol ligand (called XPEG) is added and incubated for 30 min. The idea of employing this ligand is to maximize the ligand coverage on the particles to improve their colloidal stability. Longer incubations of the XPEG ligand can lead to the replacement of thiolated DNA. The final result of the functionalization process is presented in figure 8.

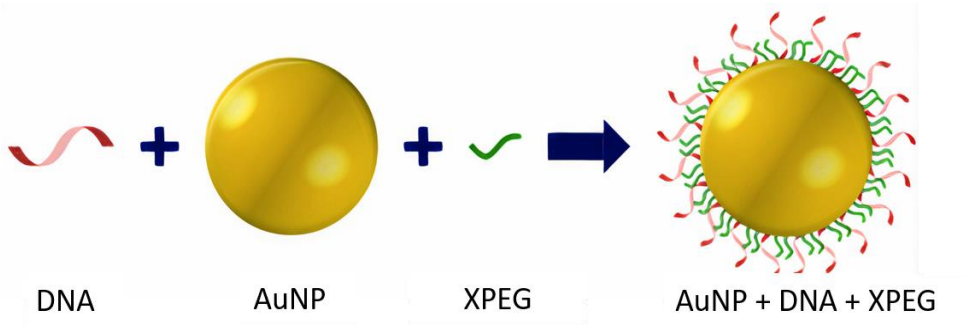

Figure 8 Gold nanosphere functionalization

The following step is the first purification through agarose electrophoresis (1% weight gel), using tris-borate-EDTA as a running buffer. Thanks to the different hydrodynamic volumes and surface charges of the functionalized particles with respect the leftover reactants and of particles that randomly aggregated following the pH treatment, it is possible to separate these different products: the leftover reactants diffuse faster in the agarose gel than the particles,

which appear as a well-defined red band (the colour due to the plasmon resonance of the particles), and which diffuse faster than aggregated particles (with a band corresponding to dimers and a trail corresponding to larger aggregates as visible in the image of figure 9a). After forty minutes of electrophoresis at 90V, it is possible to extract just the DNA functionalized gold nanospheres from the agarose gel in TBE buffer.

Subsequently, it is necessary to concentrate the sample by centrifuging it at 4° and then remove the supernatant as much as possible. At this point, the nanoparticles are mixed with the DNA origami, which was assembled and purified by agarose gel electrophoresis by our collaborators in Montpellier. In general, three samples are prepared: one with just functionalized gold particles as a reference (without DNA origami), and two with different gold nanospheres / DNA origami ratio. All samples also feature Mg^{2+} ions for the stability of the origami.

The samples are left to incubate overnight and are protected from light (to minimize bleaching the dye molecule on the origami) by covering them with aluminum foil.

On day three, the second electrophoretic purification is performed. In contrast to what is done during the second day, the process is done in a TBE running buffer, which contains $MgCl_2$, to stabilize the DNA origamis. As shown in figure 9b, we typically observe three bands in the samples featuring gold nanospheres and DNA origamis. The fastest one is composed of unreacted functionalized nanoparticles. The second one corresponds to assemblies with one nanosphere and one DNA origami (this band overlaps with non-specific aggregated dimers which also appear in the reference sample). The third line is the most interesting one with the wanted structures composed by two gold nanoparticles and one DNA origami as verified by TEM measurements performed before the beginning of my internship (see an example in figure 1b). This sample is extracted from the agarose gel and concentrated by centrifugation. At the end, 40/50 µL suspensions of gold dimers assembled by the DNA origami with a slightly pinkish colour, ready to be injected in the microfluidic chamber and analyzed in the confocal microscope.

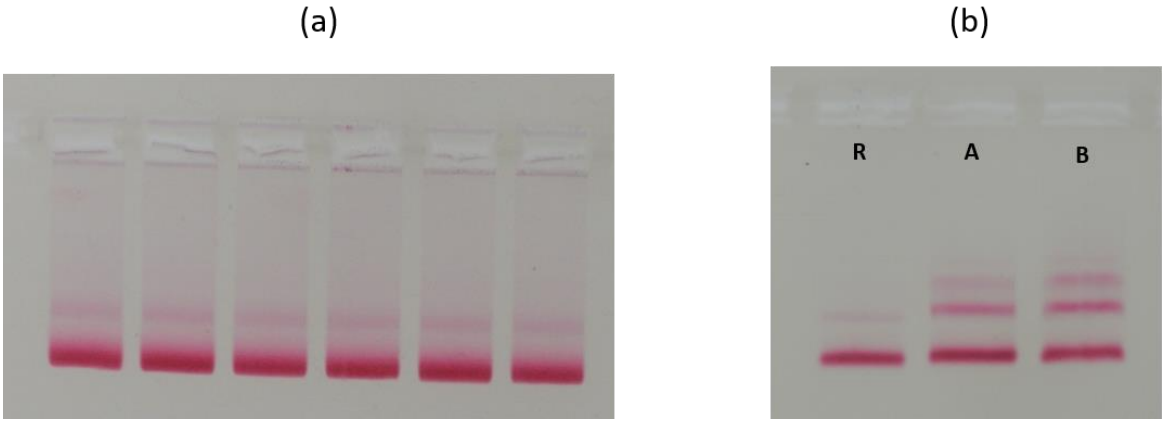

Figure 9 Electrophoresis gel (a) First purification, fastest line with single nanoparticles while the second line and the pinkish halo is basically aggregation (b) Second purification, in R there is no DNA origami and it is used as reference, in A and B there is DNA origami at different level. The fastest line is composed by single nanoparticles and bare DNA origamis. In the first line there are mainly DNA origamis with a single nanoparticle attached. In the third line there are the wanted dimers together with single nanoparticles with two DNA origamis attached, due to a similar hydrodynamic volume.

ii. Preparation of the microfluidic chambers

The aim of the microfluidic chamber is to fix single dimers on glass coverslips, while maintaining them in water to allow the *in-situ* modification of their environment (increasing the local ionic strength or injecting glycerol to increase the local refractive index). Two glass coverslips are used to have two good optical interfaces and allow transmission measurements in scattering. The idea is to functionalize the glass surfaces by injecting different proteins, which provide a specific link to the DNA origami\nanoparticles hybrid structures. Firstly, the glass slides are cleaned in an ultrasonic bath in acetone, washed with ethyl alcohol and finally subjected to ozone cleaner. This last step is crucial to avoid background fluorescence from the surface.

The microfluidic chamber structure is composed by, starting from the bottom, a back glass slide, two layers of parafilm and a front glass slide (figure 10a). The shape of the chamber is carved in the double layer of Parafilm. Between the two Parafilm layers, two narrow pipette tips (~200 µm thickness) are inserted, providing a flow chamber. The structure is baked at 105° to melt the Parafilm, which fixes the slides together. At this point, the chamber structure is ready for the functionalization with proteins (figure 10b). The first substance injected in the microfluidic chamber is BSA (bovin serum albumin) featuring biotin groups. It is an acidic protein, soluble in water, which is able to bind non-specifically to glass. The next phase is the injection of Neutravidin which binds to the biotin on BSA. In the end, a propriaritary buffer (called Superblock©) is injected in order to prevent non specific binding, which means that the sample can only bind to Neutravidin. Between each step, it is necessary to rinse the chamber with a Tris buffer solution featuring Na^+ (2 mM) and Mg^{2+} (5mM), called T5/2.

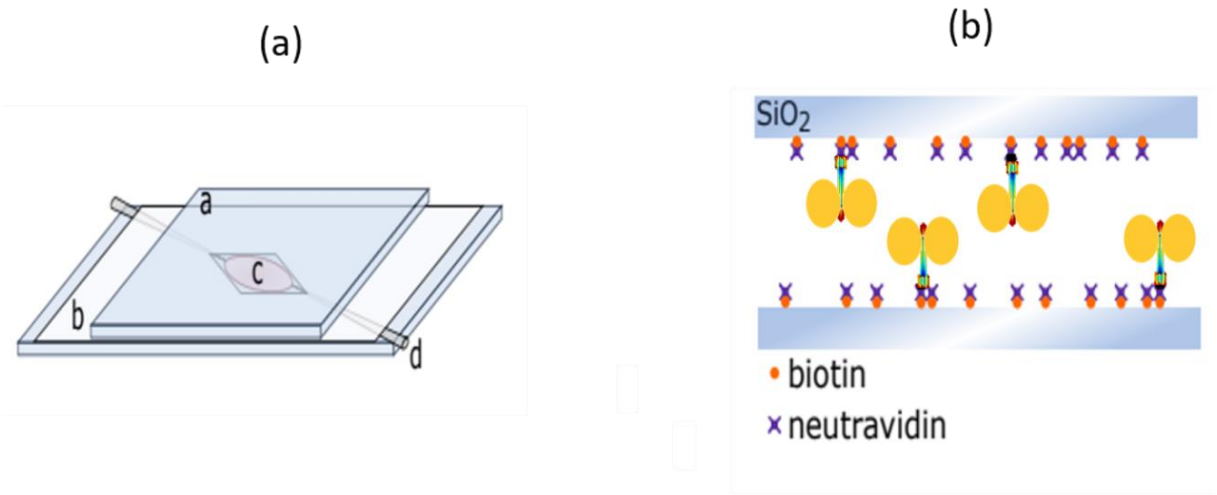

Figure 10 Microfluidic chamber (a) The structure of the chamber is showed. From the bottom: a first larger glass, two parafilm layer [b] where in between are placed the channels [d] and where is shaped the sample chamber [c], top glass [a] (b) Microfluidic chamber functionalization, with a first layer of biotin and a second layer of neutravidin where the assembled structures can be received.

At this point, the microfluidic chamber is ready to accommodate the sample. To do so, part of the the sample is diluted in T5/2 (x10) to a volume of 40µL. At this point, the assembled structures either float inside the chamber or bind the Neutravidin thanks to biotin groups

featured at the bottom of the DNA origami. Before rincing the sample with T5/2 in order to remove the unbond dimers, we observe the sample in darkfield microscopy.

iii. Experimental setup

The lifetime measurements and the spectral analysis of the plasmonic resonators are performed on the same confocal microscope (figure 11). The sample contained in the microfluidic chamber, is mounted on the piezo-controlled stage of the microscope. An objective is mounted just below the sample and in order to match the refractive index between objective and glass and in order to maximize the collection of emitted light, immersion oil is implemented. Since the purpose is to get information on lifetime but also on the spectra, it is necessary that the setup has a fast interchangeability between the different functionalities.

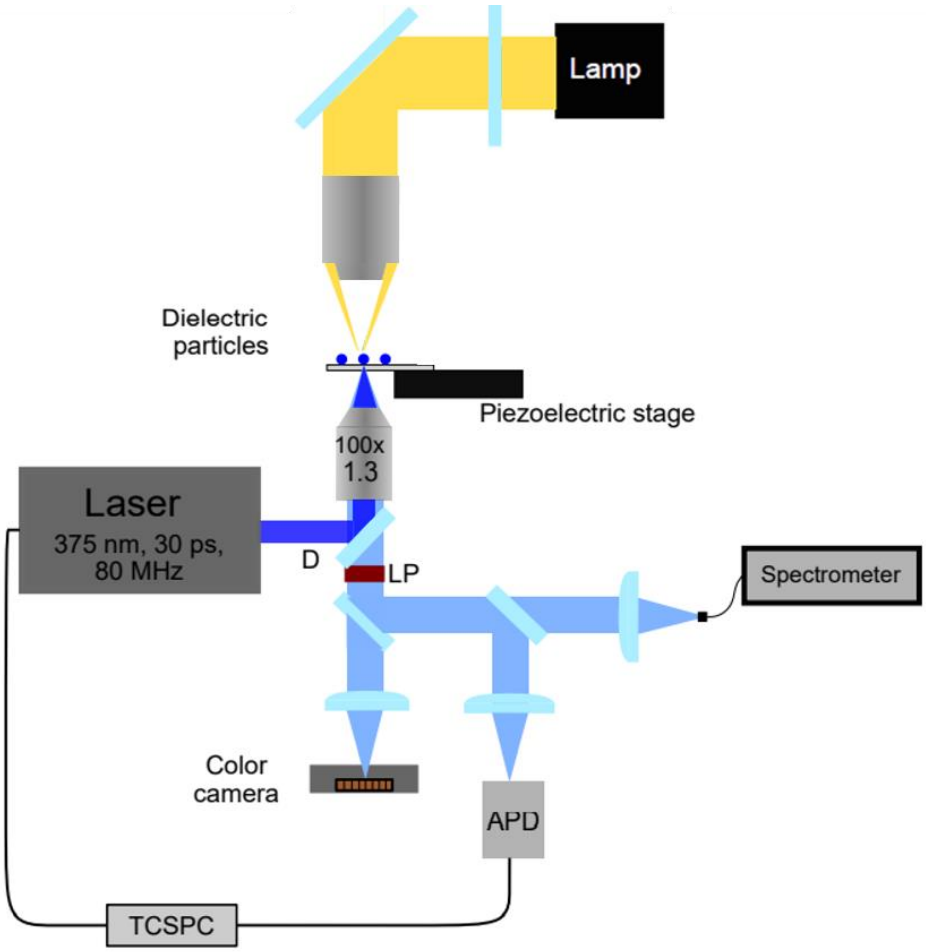

Figure 11 Confocal microscope. Darkfield image on colour camera and spectral analysis with the spectrometer performed with the halogen lamp, while lifetime analysis conducted with the laser, the TCSPC system and the APD.

In order to analyse the fluorescence signal, a 635 nm laser picosecond pulsed laser is used (TOPTICA iChrome). The beam size is increased to 10 mm to overfill the microscope objective, before going through a bandpass filter to remove unwanted frequencies of the

supercontinuum source. Subsequently, the laser beam passes through a λ/4 stage where the light is circularly polarized. Considering that the excitation dipole of the molecule inside the assembled structure can be oriented in any direction, the circular polarization of the excitation ensures that any dipole orientation can be excited. After this stage, a variable attenuator is implemented and the excitation intensity is measured on a powermeter. A lens, mounted on a flip stage, is positioned at the entrance of the microscope. When it is inserted, the laser is focused on the Fourier plane of the objective (numerical aperture – NA – of 1.3) to provide a widefield fluorescence image acquired by an EMCCD camera. When the lens is removed, the laser is focused on the sample and the fluorescence signal is measured on an avalanche photodiode (APD), which acts as a confocal pinhole to only collect photons from a single emitter. An example of time trace signal is reported in figure 12a. The time delay between the laser pulses and the photon acquisition on the APD is measured using a Time Correlated Single Photon Counting system (TCSPC). By constructing the histogram of these time delays, it is possible to infer the fluorescence lifetime of the single emitter. The analysis is performed by convoluting a single or double exponential decay function with the Instrument Response Function (IRF) of the setup (figure 12b). The latter is obtained by simply measuring the incoming laser pulses on the APD.

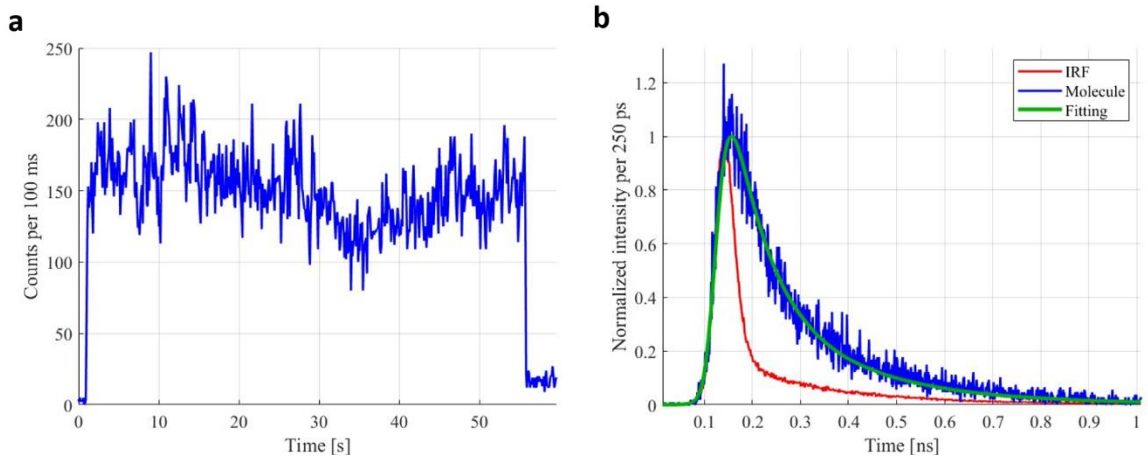

Figure 12 Lifetime analysis. a) Single molecule time trace b) Normalized intensity for lifetime analysis

Concerning the acquisition of single particle scattering spectra, it is necessary to work in darkfield microscopy. To do so, an oil immersion condenser is employed above the sample. The source of light is a halogen lamp and the incoming light impinges on the sample only at high numerical apertures (between 1.2 and 1.4). Light scattered by single nanostructures is collected by the same objective as the fluorescence signal but an iris allows the reduction of the numerical aperture to 0.55 in order to only collect scattered light and not the excitation, enhancing the contrast of the darkfield image. The darkfield image can be analysed by eye using a binocular or through a colour camera (figure 13a). By analysing the intensity and colour of the scattered light in darkfield images, it is possible to distinguish which scattering objects are dimers, monomers or larger aggregates. Using the piezoelectric stage, it is possible to save the coordinates of each scattering object and analyse them consecutively. Then, by switching a mirror, it is possible to send the signal to a fibre-coupled spectrometer and collect the scattering spectra of the single dimers since the optical fibre acts as a confocal pinhole. The final spectra are obtained with a post processing in which the noise is subtracted from the

acquired spectra before dividing the result by a normalized smooth background spectrum to correct for the wavelength dependence of the lamp and of the optical setup. An example of a spectrum of a dimer is reported in figure 13b.

During my internship I worked on analysing the scattering and fluorescence data of the assembled sample separately but also on correlating the spectral analysis with the lifetime measurements in order to associate the measured Purcell factors with the resonance wavelength of the dimer.

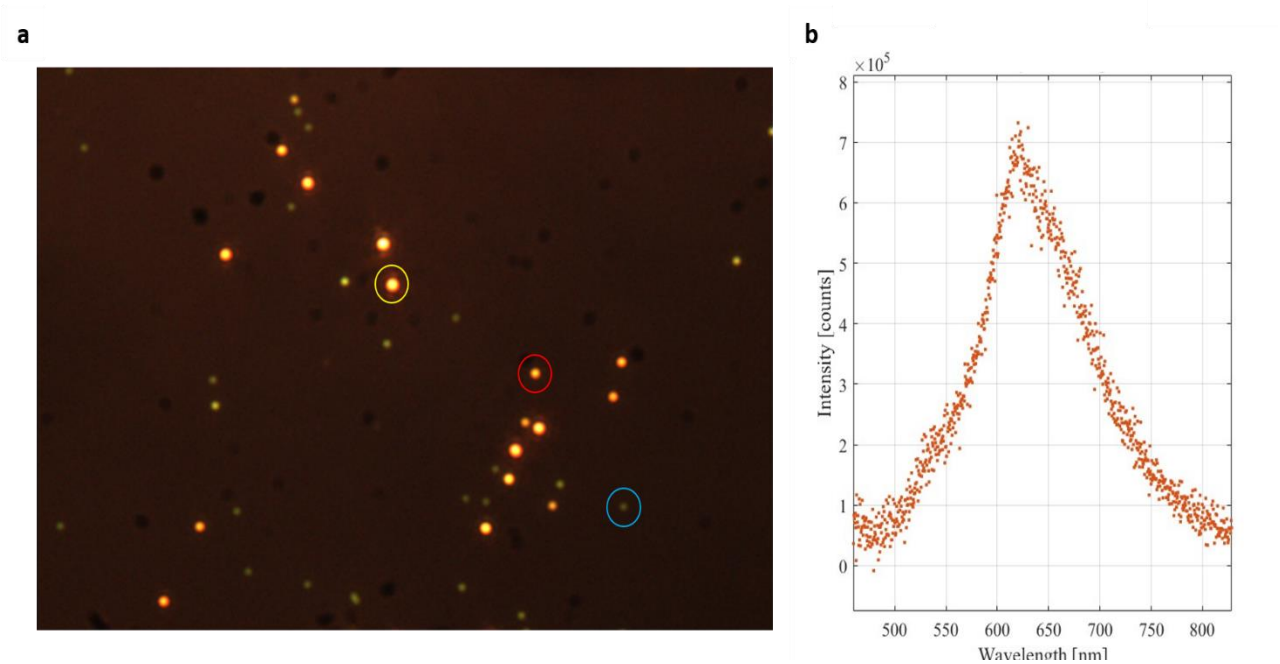

Figure 13 a) Dark field image. The white blue circled point is a monomer while the yellow circled one is an aggregation of gold nanoparticles. The red circled point is a dimer, a DNA origami attached to two gold nanoparticles b) Example of a dimer spectrum

f. Experimental results

i. Analysis of ATTO647N in DNA origamis

The spontaneous emission enhancement is related to the lifetime of the assembled structure compared to the lifetime of the bare molecule. For this purpose, we need a fluorescence lifetime reference analysis of the molecule without plasmonic resonators. Due to the absence of gold nanoparticles, we expect a long lifetime, since no resonator structure is present to amplify the spontaneous emission rate of ATTO647N. Practically, the bare sample is injected into the microfluidic chamber at low salt (T5/2) after the surface activation with BSA, Neutravidin and Superblock. The concentration of the injected DNA origami is 12.3 ng/ml. In figure 14, we can observe both a widefield image collected on the EMCCD or a confocal image inferred from the APD after piezoelectric scanning of the sample. The white spots in the EMCCD (figure 14a) image are the fluorescent molecules. In the APD scanning image (figure 14b), we have two colorbars that give more detailed information on the intensity of the signal and on the lifetime of the single molecules.

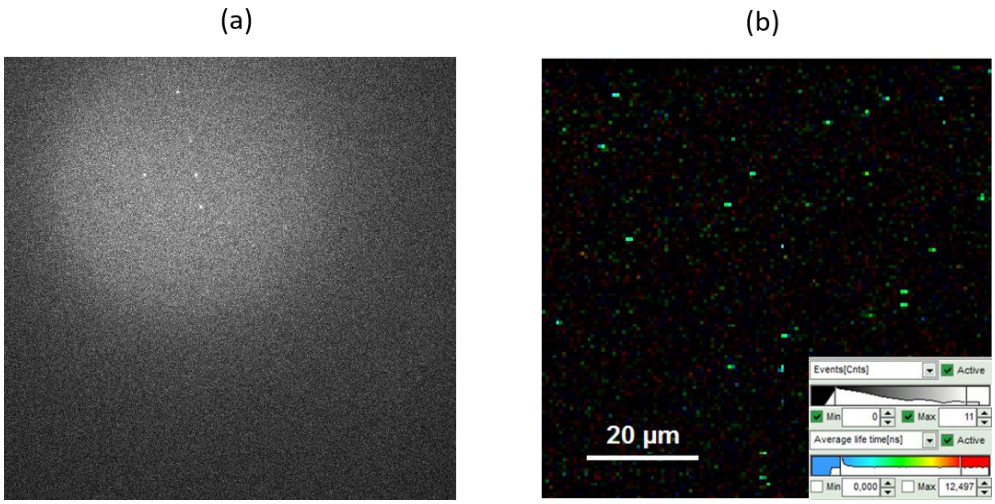

Figure 14 ATTO647N in origami images (a) EMCCD image (b) APD scanning image at 5 µW

The analysis was performed at different laser powers to check if the lifetime is power independent (figure 15a) and also to test if the fluorescence intensity reaches saturation. The lifetime values are given by the software SYMPHOTIME which performs a fit of the detected photons' arrival time with respect to the laser pulse trigger. The average lifetime of DNA origamis is 4.37 ± 0.24 ns at 5µW of laser power and 4.19 ± 0.42 ns at 10µW. But the intensities are similar for both excitations, indicating that we are close to saturation.

More information can be found by analysing the intensity with respect to the on time. The on time is essentially the surviving time of a molecule under laser excitations while the intensity tells us how many photons are collected from the APD and it is expressed in counts per seconds. In general, we observe that if the intensity of a molecule is high, the on time is shorter, as shown in figure 15b. This means that the molecules have a similar photon budget (number of photons collected before bleaching).

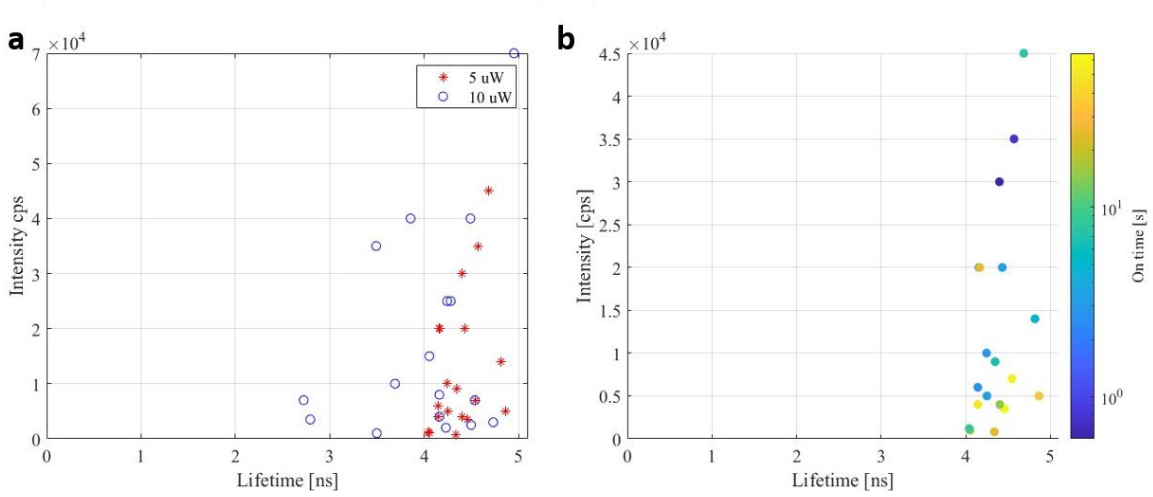

Figure 15 a) Lifetime comparison at different power laser. At 5µW less dispersed results. b) Bare molecule lifetime with respect to the intensity and the on time. In general, smaller intensities correspond to larger on time.

By looking at the time trace of a single molecule (figure 16a), it is possible to observe photoblinking, in which the emitter does not emit photons for a certain period of time but then it recovers the ability to emit again [61]. This phenomenon is linked to triplet state transitions and it is based on intersystem crossing [62] (figure 16b). From the theory, we know that a radiative transition must occur between two states with the same spin, in our case from singlet state to another singlet state. As a consequence, a transition between an excited singlet state to an intermediate triplet state is non-radiative, because of the spin parity change. The probability of a transition towards the triplet state is much lower with respect to a radiative transition and the lifetime of a molecule inside a triplet state is in the order of nanoseconds to seconds [63], explaining why we observe clear dips in the time trace. The molecule recovers the ability to emit from the ground state thanks to a second non-radiative transition from the intermediate triplet state to the ground singlet state.

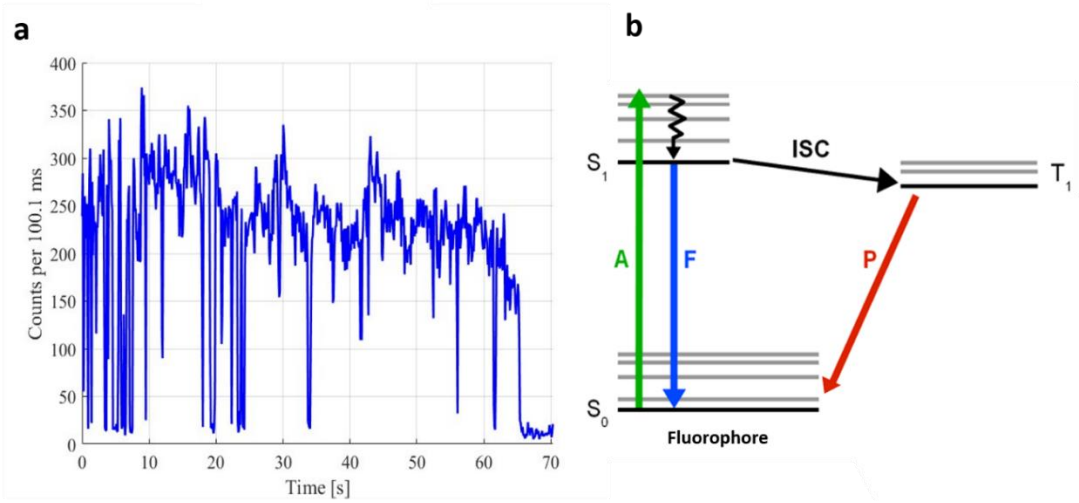

Figure 16 a) Single molecule which presents photoblinking and a final photobleaching. b) Scheme of the intersystem crossing. A non-radiative transition from the excited singlet state to an intermediate triplet state may occur with lower probability with respect to the classical singlet-singlet transition.

The transition to a triplet state plays also a role in photobleaching, the irreversible process for which a molecule loses the ability to fluoresce. In this case, the molecule in the dark triplet state does not decay in the ground singlet state but it transfers energy irreversibly to triplet oxygen, which transitions to singlet oxygen providing highly reactive oxidizing species in solution [64]. In order to limit the photoblinking and the photobleaching, it is possible to introduce photostabilizers and oxygen scavengers [65].

The lifetime results of this measurement are fruitful for the following Purcell factor calculation. Indeed, the ratio between the reference's lifetime and the dimer's lifetime is proportional to the Purcell factor.

ii. Assembled structure with 60 nm gold nanospheres

In order to enhance the spontaneous emission, we need to match the emitter frequency with the plasmonic nanostructure resonance frequency. The resonator structure is composed by two gold nanospheres and the resonance frequency is adjustable by modulating the interparticle distance. From simulations, obtained with the numerical tool MNPBEM, we can observe how by decreasing the interparticle spacing, we are able to get a large redshift in the longitudinal plasmon resonance frequency (figure 17a).

The DNA single strands on the surface of the gold nanospheres limit the minimum distance between the nanoparticles. This is due to the electrostatic and steric repulsion of the negatively charged backbone of DNA. To overcome this force, we rinse the microfluidic chamber with a solution full of positive ions which can neutralise the negative charges and collapse the DNA strands, allowing the nanospheres to get closer. Depending on the quantity of ions injected, the ionic strength of the solution changes. As a consequence, we expect that at higher ionic strengths, the nanospheres are closer (figure 17b).

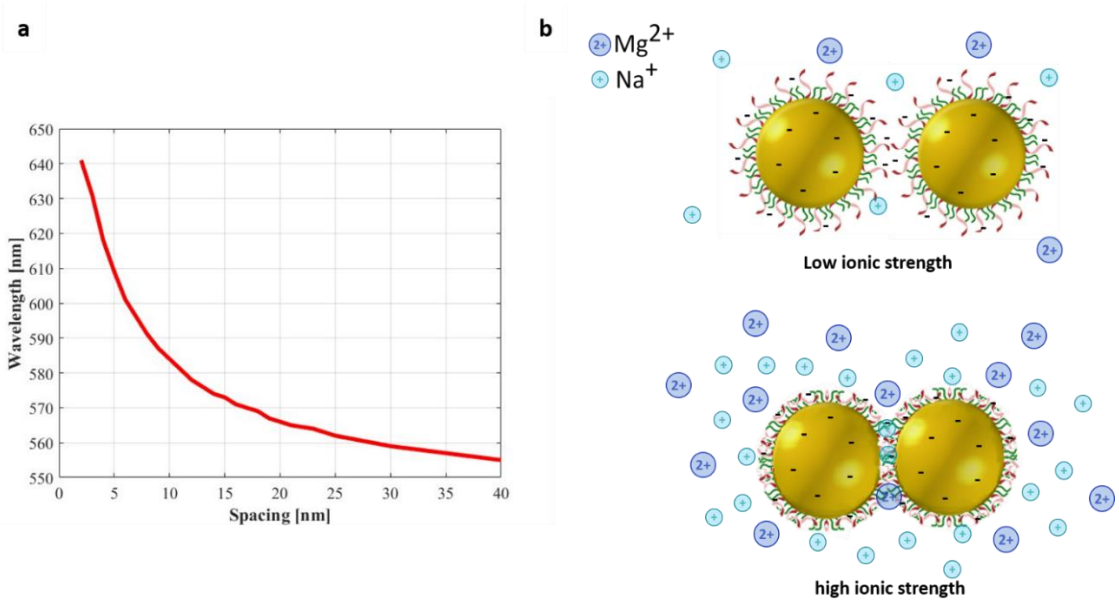

Figure 17 Interparticle distance control. a) MNPBEM simulation of two 60 nm gold nanospheres at different distances with n=1.4. Large redshift for short spacing. b) By increasing the ionic strength in the solution, the nanospheres tend to approach since the negative DNA single strands are neutralised and collapsed by the positive ions.

Experimentally, it is possible to gain the information of the plasmonic frequency by collecting the spectrum of the nanostructure as shown in the Methods section. The resonance wavelength is then fitted by a Lorentzian function. In figure 18, I report the distribution of plasmonic resonance frequencies for an ensemble of 60 nm gold nanosphere dimers at low (T5/2 with Na^+ (2 mM) and Mg^{2+} (5mM)) and at high ionic strengths (T150/500 with Na^+ (500 mM) and Mg^{2+} (150mM)). As expected, by increasing the ionic strength, we reach higher wavelengths, since the dominant mode is the longitudinal one. These kinds of measurements are performed on the same dimers, before at low ionic strength and then just by directly injecting in the chamber the high ionic strength solution. We can observe that by increasing the salt level, the dimers reach a lower distance and a consequent red shift in the longitudinal plasmonic resonance.

It is important to underline that the matching condition between spontaneous emission frequency and plasmonic resonators frequency is still far from being fulfilled. The average dimers wavelength at high ionic strength is close to 590 nm, while the resonance frequency of the fluorophore is at 647 nm.

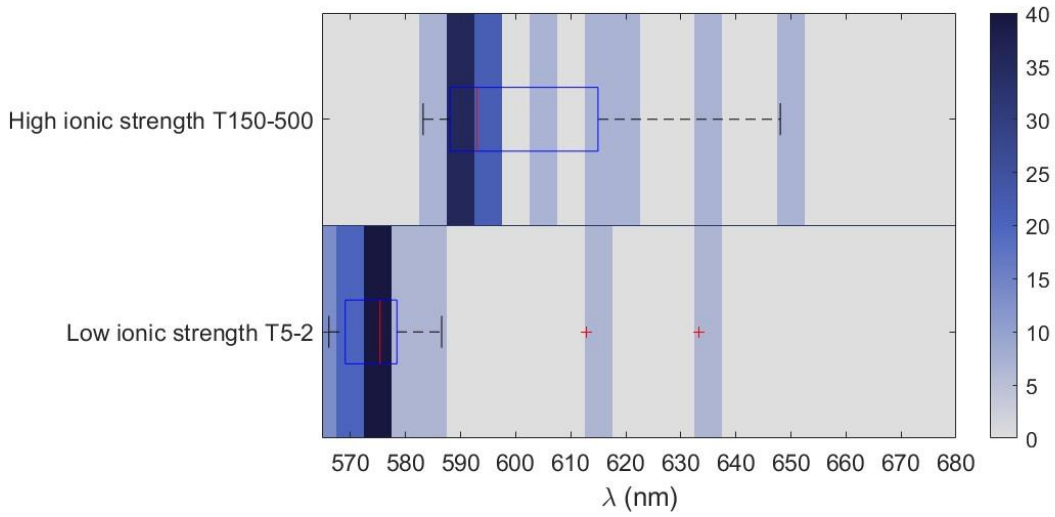

Figure 18 Plasmonic resonances of 60 nm gold dimers. By increasing the ionic strength, the frequency resonance is redshifted due to the approach of the nanospheres.

For both ionic strengths, a lifetime analysis was performed and in figure 19a are reported the results of the assembled structures, compared to the bare molecule reference lifetimes. At low ionic strength with a laser power of 15 μW, the average of the spontaneous emission lifetime is 1.02±0.60 ns with a minimum of 280 ps. The Purcell factor can be calculated as the ratio between the bare molecule's lifetime and the assembled-structure's lifetime. The average achieved factor of emission enhancement is 4, with a maximum of 15. Better values were reached for high ionic strength conditions, where the average lifetime is 293 ± 149 ps with a minimum of 75 ps. The average Purcell factor is 15 and the maximum achieved is 58. As we can see, by increasing the ionic strength, the lifetime is strongly decreased. The plasmonic resonators generate a strong electromagnetic field which provides new channels of deexcitation for the emitter. In figure 19b, we can observe a comparison between the lifetime of a bare emitter and an assembled-structure at low and high ionic strengths. The high salt one has clearly the fastest decay. In figure 19c, I provide the time trace of the fastest decay structure that I observed. As we can notice, its behavior is affected by photoblinking.

A limit of these measurements is that the data cannot be compared in terms of intensity, because the alignment was not identical when performing the reference and dimer measurements. One of the objectives of the end of my internship and of the beginning of my thesis is to perform experiments in which the intensities can be quantitatively compared.

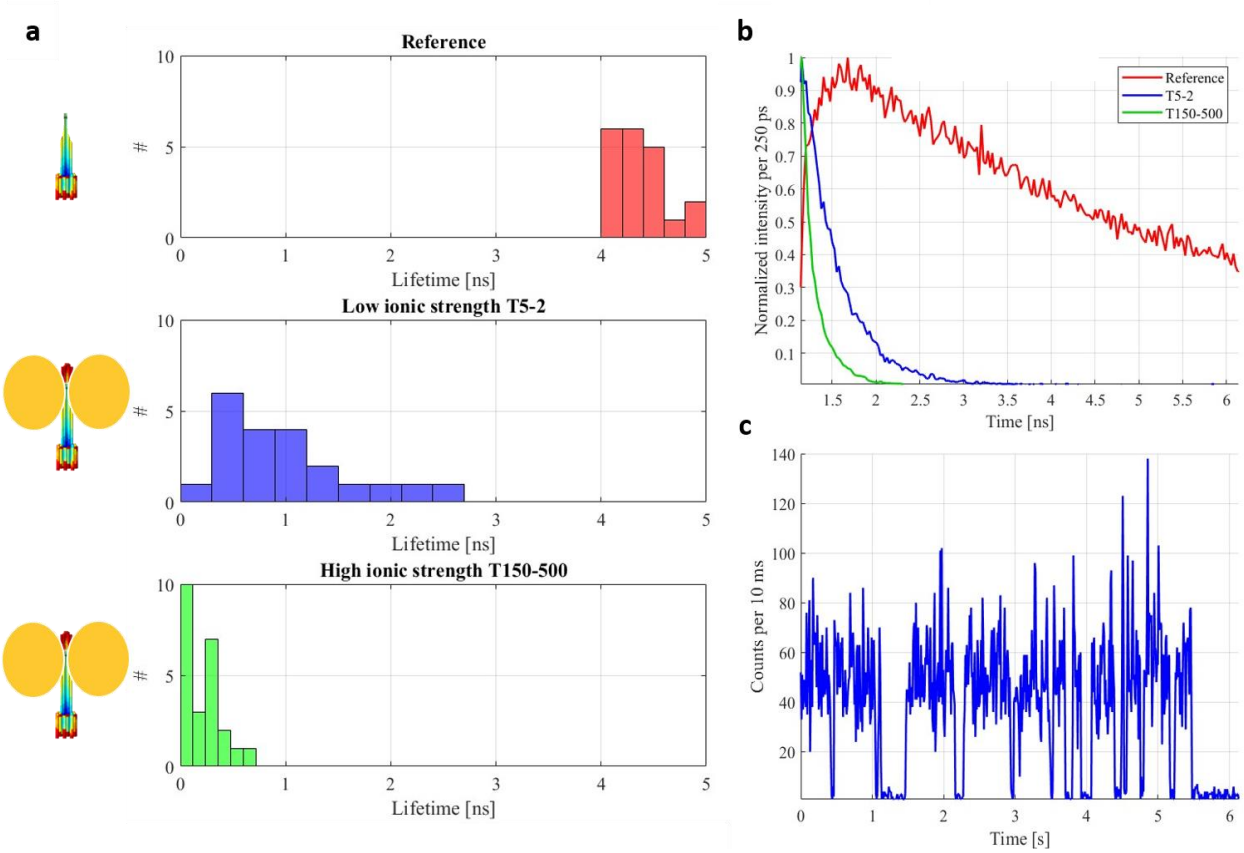

Figure 19 a) Lifetime comparison between bare molecules and assembled structures. At higher ionic strength we get shorter lifetimes. b) Lifetime measurement of bare molecule (red) and assembled structure at low ionic strength (blue) and at high ionic strength (green). c) Time trace of the shortest lifetime structure observed at high ionic strength.

iii. Increasing the refractive index of the environment

The frequency matching condition even at high ionic strengths is not reached. To push the plasmonic resonance at higher wavelengths, one possibility is to change the refractive index of the environment [66]. By adding a solution with a certain concentration of glycerol, the electromagnetic environment around the assembled structure changes. According to the quasistatic approximation described in the theory section, for a single sphere, the resonance condition is $\mathrm{Re}(\varepsilon_p) = -2\varepsilon_{ext}$. And since the real part of the refractive index of gold decreases for larger wavelengths (figure4a), if ε_{ext} increases then the resonance redshifts. During my internship, I investigated how the plasmonic resonances shift at high ionic strengths when adding solutions at 50%, 60% and 80% of glycerol. As we can see from figure 20, the longitudinal resonance frequencies are clearly shifted towards the red part of the spectrum

by increasing the glycerol concentration. From these kinds of environments, we expect strong enhancement of the fluorescence. I am currently investigating the fluorescence enhancement of ATTO647N in dimers in glycerol solutions while trying to ensure comparable conditions to a reference measurement for a quantitative analysis of intensity enhancements.

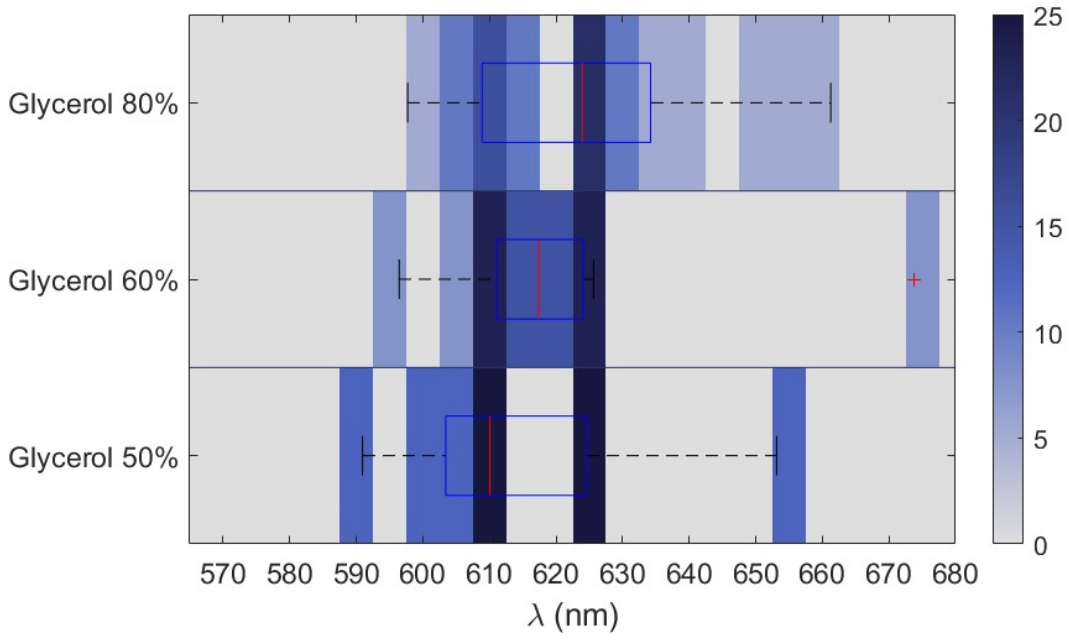

Figure 20 Distribution of plasmonic resonance frequencies from single 60 nm nanosphere dimers at high ionic strengths for different concentrations of glycerol.

iv. Correlated measurements

In parallel to the studies described above, I worked during my internship on correlating the lifetime and spectral measurements on the same nanostructures. Indeed, the previous studies were performed on the same samples but without looking at the same nanostructures: they provide statistical information on the sample but it is not possible to verify whether the highest Purcell factors are achieved by the dimers with resonances close to 650 nm. In a first step, I tried simply to correlate the APD scanning images with the darkfield image, but recognizing the patterns was non-trivial. The two images were difficult to compare because the image scales were different and also because not all the items that fluoresce also feature a detectable scattering signal (for instance origamis from which the nanospheres detached), and vice versa (dimers in which the ATTO647N bleached prior to the measurement).

The solution we chose was to use the darkfield image to distinguish, from the intensity of the spot and by the colour of the scattered light, if a structure is a monomer or a dimer. By moving the piezo electric stage, we can position the scatterer in the confocal measurement volume and either collect its scattering response on the spectrometer through the fibre (which gives us quantitative information on the plasmon resonance wavelength and further ensures that the object is a dimer or monomer) or collect its fluorescence under laser excitation on the APD. To perform this correlation, the issue is to ensure that the confocal volume corresponding to the 50 µm wide APD is perfectly superimposed with the confocal volume of

the 100 µm wide fibre of the spectrometer and with the laser focus. This also requires that the sample plane is conjugated to the APD, to the fibre and to both cameras (colour and EMCCD) by the microscope objective. I therefore worked extensively on the alignment of the confocal microscope to ensure these conditions.

Figure 21 shows a first example of such correlated measurements in which I provide the scattering response and correlated lifetime measurement on a monomer and a dimer of 60 nm nanospheres, using a sample at high ionic strength. The dimer structure presents a redshift in plasmonic resonance and also an increase of the scattering signal with respect to the monomer. We observe that the fluorescence lifetime measured with the dimer is significantly shorter than with the monomer, as expected from the increased LDOS.

The interest of correlating plasmon resonance spectra and lifetime measurements goes beyond the ability to associate large Purcell factors to specific dimer resonance conditions. Indeed, this setup also allows the measurement of the resonance spectra before and after studying the lifetime and observing the emitter photobleach. It is therefore very interesting if the Purcell factor is sufficient to go from weak to strong coupling, leading to the hybridization of the emitter and cavity resonances. Such strong coupling regimes were recently observed between gold nanostructures and several fluorescent molecules [67] and, in particular, in DNA-linked gold particle dimers in the group of S. Bidault [53]. By analysing the resonances before and after bleaching, it is possible to verify that the hybridized modes disappear without the molecules and were indeed due to a strong coupling process [53]. Overall, during my PhD, I will generalize this correlated measurement scheme to achieve a broader understanding of the coupling mechanisms between quantum emitters and plasmonic resonators.

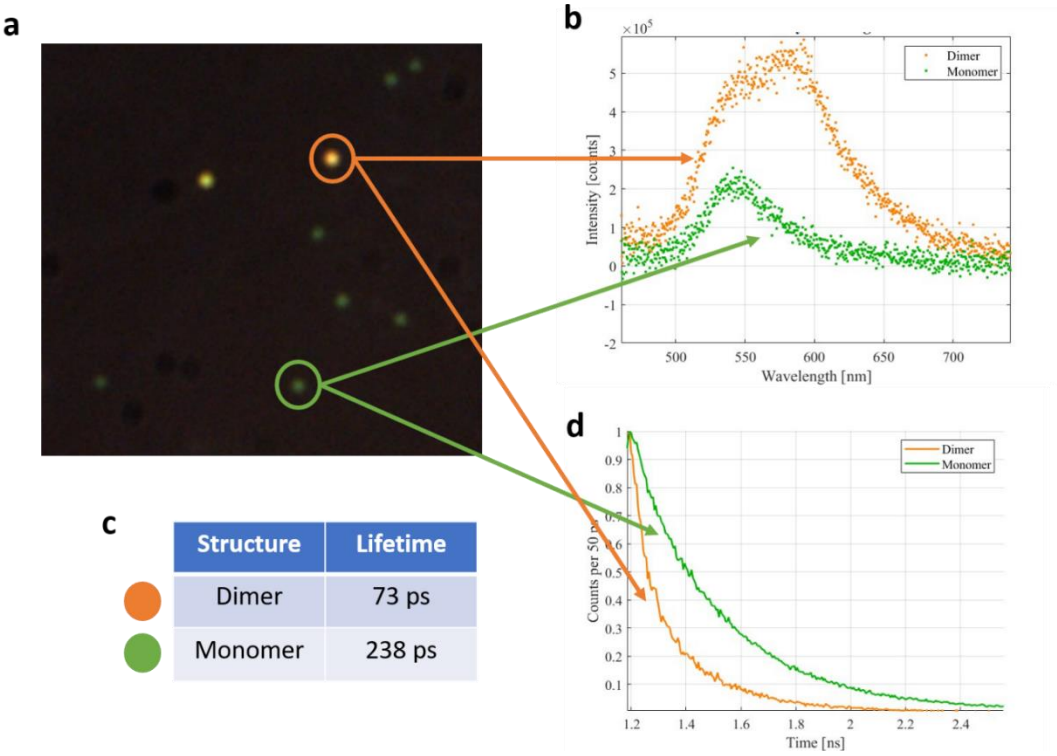

Figure 21 Example of correlated measurement performed on a dimer (orange) and on a monomer (green) a) Darkfield image b) Acquired spectra c) Lifetime values d) Exponential decays

g. Conclusions and future perspectives

The enhancement of spontaneous emission is essential for fast quantum communication systems. At room temperature it is not just an advantage, but it is also a requirement, since we need to ensure a decay rate higher than phonon-induced dephasing. The highest Purcell factor that I gained is 50 at high ionic strength. It is still far from the required 10^5, but many things could be done in the future. The first thing is to finalize fluorescence lifetime measurements at high refractive indices. A second step is to develop a DNA origami which allows the control over the orientation of the molecular dipole to keep it parallel to the dimer axis and maximise the spontaneous emission of the dye.

To go further, it is possible to use nanocubes which exploit the lightning rod effect on the tips with a significant electromagnetic field enhancement. Moreover, it has been theoretically demonstrated by our group [52] that strong coupling regime is reachable for dimers of nanocubes coupled to a single molecule. In strong coupling, we have the hybridization of the plasmonic mode with the resonance of the emitter, leading to coherent coupling. This hybridization leads to the formation of new quasiparticles called polaritons. A key signature of strong coupling is the splitting of the original resonance frequencies into two distinct peaks. This phenomenon, known as mode splitting, allows the system to exhibit two stable states for a single input light intensity, a property called bistability [68]. This feature opens the doors to advanced applications such as optical switches [69] and optical memories [70].

For indistinguishable single photons at room temperature, we need slightly lower Purcell factors to remain in weak coupling while beating dephasing [71]. A second solution in this case is to produce emitters with slower dephasing and increased transition dipoles. This is possible by coupling several emitters in a strong coupling regime (so-called J-aggregates) [72], similarly to what is performed in photosynthesis pigments. This is the second direction of my PhD project: optimizing emitter-resonator coupling by optimizing the emitter properties. This will be done by mimicking photosynthetic pigments with DNA origamis in order to produce emitters with larger emission dipoles and slower dephasing times.

h. Bibliography

[1] J. Vuckovic, D. Fattal, C. Santori, G. Solomon, and Y. Yamamoto, 'Enhanced single-photon emission from a quantum dot in a micropost microcavity', *Appl. Phys. Lett.*, vol. 82, Jul. 2003, doi: 10.1063/1.1577828.

[2] T. Heindel, J.-H. Kim, N. Gregersen, A. Rastelli, and S. Reitzenstein, *Quantum dots for photonic quantum information technology*. 2023.

[3] R. Brouri, A. Beveratos, J.-P. Poizat, and P. Grangier, 'Photon antibunching in the fluorescence of individual color centers in diamond', *Opt. Lett.*, vol. 25, no. 17, pp. 1294–1296, Sep. 2000, doi: 10.1364/OL.25.001294.

[4] M. Hijlkema, B. Weber, H. P. Specht, S. C. Webster, A. Kuhn, and G. Rempe, 'A single-photon server with just one atom', *Nat. Phys.*, vol. 3, no. 4, pp. 253–255, Apr. 2007, doi: 10.1038/nphys569.

[5] C. L. Morrison *et al.*, 'Single-emitter quantum key distribution over 175 km of fibre with optimised finite key rates', *Nat. Commun.*, vol. 14, no. 1, p. 3573, Jun. 2023, doi: 10.1038/s41467-023-39219-5.

[6] M. J. Holmes and Y. Arakawa, 'The heat is on: towards the realization of non-cryogenic photonic quantum technologies', *Mater. Quantum Technol.*, vol. 1, no. 1, p. 013001, Mar. 2021, doi: 10.1088/2633-4356/abb07e.

[7] T. T. H. Do *et al.*, 'Room-temperature strong coupling in a single-photon emitter-metasurface system', *Nat. Commun.*, vol. 15, no. 1, p. 2281, Mar. 2024, doi: 10.1038/s41467-024-46544-w.

[8] H. Siampour *et al.*, 'Observation of large spontaneous emission rate enhancement of quantum dots in a broken-symmetry slow-light waveguide', *Npj Quantum Inf.*, vol. 9, no. 1, pp. 1–8, Feb. 2023, doi: 10.1038/s41534-023-00686-9.

[9] A. F. Koenderink, 'On the use of Purcell factors for plasmon antennas', *Opt. Lett.*, vol. 35, no. 24, pp. 4208–4210, Dec. 2010, doi: 10.1364/OL.35.004208.

[10] T. V. Raziman and O. J. F. Martin, 'Orientation Dependence of Plasmonically Enhanced Spontaneous Emission', *J. Phys. Chem. C*, vol. 120, no. 37, pp. 21037–21046, Sep. 2016, doi: 10.1021/acs.jpcc.6b03297.

[11] A. Konrad, M. Metzger, A. M. Kern, M. Brecht, and A. J. Meixner, 'Revealing the radiative and non-radiative relaxation rates of the fluorescent dye Atto488 in a λ /2 Fabry–Pérot-resonator by spectral and time resolved measurements', *Nanoscale*, vol. 8, no. 30, pp. 14541–14547, 2016, doi: 10.1039/C6NR02380K.

[12] M. Y. Berezin and S. Achilefu, 'Fluorescence Lifetime Measurements and Biological Imaging', *Chem. Rev.*, vol. 110, no. 5, pp. 2641–2684, May 2010, doi: 10.1021/cr900343z.

[13] W. E. Moerner and M. Orrit, 'Illuminating Single Molecules in Condensed Matter', *Science*, vol. 283, no. 5408, pp. 1670–1676, Mar. 1999, doi: 10.1126/science.283.5408.1670.

[14] W. Peng, J.-W. Zhou, M.-L. Li, L. Sun, Y.-J. Zhang, and J.-F. Li, 'Construction of nanoparticle-on-mirror nanocavities and their applications in plasmon-enhanced spectroscopy', *Chem. Sci.*, vol. 15, no. 8, pp. 2697–2711, 2024, doi: 10.1039/D3SC05722D.

[15] M. Sovizi and M. Aliannezhadi, 'Localized surface plasmon resonance (LSPR) of coupled metal nanospheres in longitudinal, transverse and three-dimensional coupling configurations', *Optik*, vol. 252, p. 168518, Feb. 2022, doi: 10.1016/j.ijleo.2021.168518.

[16] M. Locarno and D. Brinks, 'Analytical calculation of plasmonic resonances in metal nanoparticles: A simple guide', *Am. J. Phys.*, vol. 91, no. 7, p. 538, Jul. 2023, doi: 10.1119/5.0094967.

[17] L. Tao, S. Deng, H. Gao, H. Lv, X. Wen, and M. Li, 'Experimental Investigation of the Dielectric Constants of Thin Noble Metallic Films Using a Surface Plasmon Resonance Sensor', *Sensors*, vol. 20, no. 5, p. 1505, Mar. 2020, doi: 10.3390/s20051505.

[18] P. B. Johnson and R. W. Christy, 'Optical Constants of the Noble Metals', *Phys. Rev. B*, vol. 6, no. 12, pp. 4370–4379, 1972.

[19] J. J. Mock, R. T. Hill, A. Degiron, S. Zauscher, A. Chilkoti, and D. R. Smith, 'Distance-Dependent Plasmon Resonant Coupling between a Gold Nanoparticle and Gold Film', *Nano Lett.*, vol. 8, no. 8, pp. 2245–2252, Aug. 2008, doi: 10.1021/nl080872f.

[20] 'Mie theory and the dichroic effect for spherical gold nanoparticles: an experimental approach', *Nanoscale Adv.*, vol. 3, no. 12, pp. 3530–3536, Jun. 2021, doi: 10.1039/d1na00148e.

[21] G. Mie, 'Contributions to the optics of turbid media, particularly of colloidal metal solutions', *Ann. Phys.*, vol. 330, pp. 377–445, 1908.

[22] U. Hohenester, 'Simulating electron energy loss spectroscopy with the MNPBEM toolbox', *Comput. Phys. Commun.*, vol. 185, no. 3, pp. 1177–1187, 2014.

[23] U. Hohenester and A. Trügler, 'MNPBEM – A Matlab toolbox for the simulation of plasmonic nanoparticles', *Comput. Phys. Commun.*, vol. 183, no. 2, pp. 370–381, 2012.

[24] J. Waxenegger, A. Trügler, and U. Hohenester, 'Plasmonics simulations with the MNPBEM toolbox: Consideration of substrates and layer structures', *Comput. Phys. Commun.*, vol. 193, pp. 138–150, 2015.

[25] A. Movsesyan *et al.*, 'Hybridization and Dehybridization of Plasmonic Modes', *J. Phys. Chem. C*, vol. 125, no. 1, pp. 724–731, Jan. 2021, doi: 10.1021/acs.jpcc.0c08570.

[26] G. Baffou and R. Quidant, 'Nanoplasmonics for chemistry', *Chem. Soc. Rev.*, vol. 43, no. 11, pp. 3898–3907, 2014.

[27] E. Hao and G. C. Schatz, 'Electromagnetic fields around silver nanoparticles and dimers', *J. Chem. Phys.*, vol. 120, no. 1, pp. 357–366, Jan. 2004, doi: 10.1063/1.1629280.

[28] T. Neuman, R. Esteban, D. Casanova, F. J. García-Vidal, and J. Aizpurua, 'Coupling of Molecular Emitters and Plasmonic Cavities beyond the Point-Dipole Approximation', *Nano Lett.*, vol. 18, no. 4, pp. 2358–2364, Apr. 2018, doi: 10.1021/acs.nanolett.7b05297.

[29] S. Cao, Y. Xing, Y. Sun, Z. Liu, and S. He, 'Strong Coupling between a Single Quantum Emitter and a Plasmonic Nanoantenna on a Metallic Film', *Nanomaterials*, vol. 12, no. 9, Art. no. 9, Jan. 2022, doi: 10.3390/nano12091440.

[30] L. Deák and T. Fülöp, 'Reciprocity in quantum, electromagnetic and other wave scattering', *Ann. Phys.*, vol. 327, no. 4, pp. 1050–1077, Apr. 2012, doi: 10.1016/j.aop.2011.10.013.

[31] L. Novotny and N. van Hulst, 'Antennas for light', *Nat. Photonics*, vol. 5, no. 2, pp. 83–90, 2011.

[32] D. Cao *et al.*, 'Mapping the Radiative and the Apparent Nonradiative Local Density of States in the Near Field of a Metallic Nanoantenna', *ACS Photonics*, vol. 2, no. 2, pp. 189–193, 2015.

[33] K. H. Drexhage, 'Influence of a dielectric interface on fluorescence decay time', *J. Lumin.*, vol. 1–2, pp. 693–701, 1970.

[34] S. Kühn, U. Håkanson, L. Rogobete, and V. Sandoghdar, 'Enhancement of Single-Molecule Fluorescence Using a Gold Nanoparticle as an Optical Nanoantenna', *Phys. Rev. Lett.*, vol. 97, no. 1, p. 017402, 2006.

[35] P. Anger, P. Bharadwaj, and L. Novotny, 'Enhancement and Quenching of Single-Molecule Fluorescence', *Phys. Rev. Lett.*, vol. 96, no. 11, p. 113002, 2006.

[36] A. Kinkhabwala, Z. Yu, S. Fan, Y. Avlasevich, K. Müllen, and W. E. Moerner, 'Large single-molecule fluorescence enhancements produced by a bowtie nanoantenna', *Nat. Photonics*, vol. 3, pp. 654–657, 2009.

[37] A. G. Curto, T. H. Taminiau, G. Volpe, M. P. Kreuzer, R. Quidant, and N. F. van Hulst, 'Multipolar radiation of quantum emitters with nanowire optical antennas', *Nat. Commun.*, vol. 4, no. 1, p. 1750, 2013.

[38] A. G. Curto, G. Volpe, T. H. Taminiau, M. P. Kreuzer, R. Quidant, and N. F. van Hulst, 'Unidirectional Emission of a Quantum Dot Coupled to a Nanoantenna', *Science*, 2010.

[39] J. Seelig *et al.*, 'Nanoparticle-Induced Fluorescence Lifetime Modification as Nanoscopic Ruler: Demonstration at the Single Molecule Level', *Nano Lett.*, vol. 7, no. 3, pp. 685–689, 2007.

[40] J. Zhang, Y. Fu, M. H. Chowdhury, and J. R. Lakowicz, 'Metal-Enhanced Single-Molecule Fluorescence on Silver Particle Monomer and Dimer: Coupling Effect between Metal Particles', *Nano Lett.*, vol. 7, no. 7, pp. 2101–2107, 2007.

[41] M. P. Busson, B. Rolly, B. Stout, N. Bonod, and S. Bidault, 'Accelerated single photon emission from dye molecule-driven nanoantennas assembled on DNA', *Nat. Commun.*, vol. 3, no. 1, pp. 1–6, 2012.

[42] S. Bidault *et al.*, 'Picosecond Lifetimes with High Quantum Yields from Single-Photon-Emitting Colloidal Nanostructures at Room Temperature', *ACS Nano*, vol. 10, no. 4, pp. 4806–4815, Apr. 2016, doi: 10.1021/acsnano.6b01729.

[43] G. P. Acuna, F. M. Möller, P. Holzmeister, S. Beater, B. Lalkens, and P. Tinnefeld, 'Fluorescence Enhancement at Docking Sites of DNA-Directed Self-Assembled Nanoantennas', *Science*, vol. 338, no. 6106, pp. 506–510, 2012.

[44] A. Puchkova *et al.*, 'DNA Origami Nanoantennas with over 5000-fold Fluorescence Enhancement and Single-Molecule Detection at 25 µM', *Nano Lett.*, vol. 15, pp. 8354–8359, 2015.

[45] L. Xin *et al.*, 'Watching a Single Fluorophore Molecule Walk into a Plasmonic Hotspot', *ACS Photonics*, vol. 6, no. 4, pp. 985–993, 2019.

[46] K. Trofymchuk *et al.*, 'Addressable nanoantennas with cleared hotspots for single-molecule detection on a portable smartphone microscope', *Nat. Commun.*, vol. 12, no. 1, p. 950, 2021.

[47] 'Recent Advances in DNA Origami-Engineered Nanomaterials and Applications | Chemical Reviews'. Accessed: Jun. 12, 2024. [Online]. Available: https://pubs.acs.org/doi/10.1021/acs.chemrev.3c00028

[48] J. Bush, S. Singh, M. Vargas, E. Oktay, C.-H. Hu, and R. Veneziano, 'Synthesis of DNA Origami Scaffolds: Current and Emerging Strategies', *Molecules*, vol. 25, no. 15, p. 3386, Jul. 2020, doi: 10.3390/molecules25153386.

[49] 'Fabricating higher-order functional DNA origami structures to reveal biological processes at multiple scales | NPG Asia Materials'. Accessed: Jun. 12, 2024. [Online]. Available: https://www.nature.com/articles/s41427-023-00470-3

[50] L. Li, S. Nie, T. Du, J. Zhao, and X. Chen, 'DNA origami technology for biomedical applications: Challenges and opportunities', *MedComm – Biomater. Appl.*, vol. 2, no. 2, p. e37, 2023, doi: 10.1002/mba2.37.

[51] 'DNA Origami-Enabled Plasmonic Sensing | The Journal of Physical Chemistry C'. Accessed: Jun. 12, 2024. [Online]. Available: https://pubs.acs.org/doi/10.1021/acs.jpcc.0c11238

[52] J. Heintz, F. Legittimo, and S. Bidault, 'Dimers of Plasmonic Nanocubes to Reach Single-Molecule Strong Coupling with High Emission Yields', *J. Phys. Chem. Lett.*, vol. 13, no. 51, pp. 11996–12003, Dec. 2022, doi: 10.1021/acs.jpclett.2c02872.

[53] J. Heintz, N. Markešević, E. Y. Gayet, N. Bonod, and S. Bidault, 'Few-Molecule Strong Coupling with Dimers of Plasmonic Nanoparticles Assembled on DNA', *ACS Nano*, vol. 15, no. 9, pp. 14732–14743, Sep. 2021, doi: 10.1021/acsnano.1c04552.

[54] S. Pal, Z. Deng, H. Wang, S. Zou, Y. Liu, and H. Yan, 'DNA Directed Self-Assembly of Anisotropic Plasmonic Nanostructures', *J. Am. Chem. Soc.*, vol. 133, no. 44, pp. 17606–17609, Nov. 2011, doi: 10.1021/ja207898r.

[55] A. K. Adamczyk *et al.*, 'DNA Self-Assembly of Single Molecules with Deterministic Position and Orientation', *ACS Nano*, vol. 16, no. 10, pp. 16924–16931, Oct. 2022, doi: 10.1021/acsnano.2c06936.

[56] L. L. Ong *et al.*, 'Programmable self-assembly of three-dimensional nanostructures from 10,000 unique components', *Nature*, vol. 552, no. 7683, pp. 72–77, Dec. 2017, doi: 10.1038/nature24648.

[57] A. Mills *et al.*, 'A modular spring-loaded actuator for mechanical activation of membrane proteins', *Nat. Commun.*, vol. 13, no. 1, p. 3182, Jul. 2022, doi: 10.1038/s41467-022-30745-2.

[58] M. Rueda, F. Prieto, J. Álvarez-Malmagro, and A. Rodes, 'Evidences of adenine–thymine Interactions at gold electrodes interfaces as provided by in-situ infrared spectroscopy', *Electrochem. Commun.*, vol. 35, pp. 53–56, Oct. 2013, doi: 10.1016/j.elecom.2013.07.026.

[59] Z. Li, R. Jin, C. A. Mirkin, and R. L. Letsinger, 'Multiple thiol-anchor capped DNA–gold nanoparticle conjugates', *Nucleic Acids Res.*, vol. 30, no. 7, pp. 1558–1562, 2002.

[60] T. Gao, W. Zhang, Y. Wang, and G. Yang, 'DNA Compaction and Charge Neutralization Regulated by Divalent Ions in very Low pH Solution', *Polymers*, vol. 11, no. 2, p. 337, Feb. 2019, doi: 10.3390/polym11020337.

[61] J. Schuster, J. Brabandt, and C. von Borczyskowski, 'Discrimination of photoblinking and photobleaching on the single molecule level', *J. Lumin.*, vol. 127, no. 1, pp. 224–229, Nov. 2007, doi: 10.1016/j.jlumin.2007.02.028.

[62] M. Vogel, A. Gruber, J. Wrachtrup, and C. von Borczyskowski, 'Determination of Intersystem Crossing Parameters via Observation of Quantum Jumps on Single Molecules', *J. Phys. Chem.*, vol. 99, no. 41, pp. 14915–14917, Oct. 1995, doi: 10.1021/j100041a003.

[63] J. Veerman, M. Parajo, L. Kuipers, and N. Van Hulst, 'Time-Varying Triplet State Lifetimes of Single Molecules', *Phys. Rev. Lett. - PHYS REV LETT*, vol. 83, pp. 2155–2158, Sep. 1999, doi: 10.1103/PhysRevLett.83.2155.

[64] D. Cooper, H. Uhm, L. J. Tauzin, N. Poddar, and C. F. Landes, 'Photobleaching Lifetimes of Cyanine Fluorophores Used for Single Molecule Förster Resonance Energy Transfer in the Presence of Various Photoprotection Systems', *Chembiochem Eur. J. Chem. Biol.*, vol. 14, no. 9, p. 10.1002/cbic.201300030, Jun. 2013, doi: 10.1002/cbic.201300030.

[65] M. Kümmerlin, A. Mazumder, and A. N. Kapanidis, 'Bleaching-resistant, Near-continuous Single-molecule Fluorescence and FRET Based on Fluorogenic and Transient DNA Binding', *ChemPhysChem*, vol. 24, no. 12, p. e202300175, 2023, doi: 10.1002/cphc.202300175.

[66] I. Tanabe, Y. Y. Tanaka, K. Watari, W. Inami, Y. Kawata, and Y. Ozaki, 'Enhanced Surface Plasmon Resonance Wavelength Shifts by Molecular Electronic Absorption in Far- and Deep-Ultraviolet Regions', *Sci. Rep.*, vol. 10, no. 1, p. 9938, Jun. 2020, doi: 10.1038/s41598-020-66949-z.

[67] R. Chikkaraddy *et al.*, 'Single-molecule strong coupling at room temperature in plasmonic nanocavities', *Nature*, vol. 535, pp. 127–130, 2016.

[68] A. Dombi, A. Vukics, and P. Domokos, 'Optical bistability in strong-coupling cavity QED with a few atoms', *J. Phys. B At. Mol. Opt. Phys.*, vol. 46, no. 22, p. 224010, Nov. 2013, doi: 10.1088/0953-4075/46/22/224010.

[69] D. E. Chang, A. S. Sørensen, E. A. Demler, and M. D. Lukin, 'A single-photon transistor using nano-scale surface plasmons', *Nat. Phys.*, vol. 3, no. 11, pp. 807–812, Nov. 2007, doi: 10.1038/nphys708.

[70] Y. Lei, F. K. Asadi, T. Zhong, A. Kuzmich, C. Simon, and M. Hosseini, 'Quantum optical memory for entanglement distribution', *Optica*, vol. 10, no. 11, pp. 1511–1528, Nov. 2023, doi: 10.1364/OPTICA.493732.

[71] I. M. Palstra, H. M. Doeleman, and A. F. Koenderink, 'Hybrid cavity-antenna systems for quantum optics outside the cryostat?', *Nanophotonics*, vol. 8, no. 9, pp. 1513–1531, Sep. 2019, doi: 10.1515/nanoph-2019-0062.

[72] D. Melnikau, P. Samokhvalov, A. Sánchez-Iglesias, M. Grzelczak, I. Nabiev, and Y. P. Rakovich, 'Strong coupling effects in a plexciton system of gold nanostars and J-aggregates', *J. Lumin.*, vol. 242, p. 118557, Feb. 2022, doi: 10.1016/j.jlumin.2021.118557.